Nanoscale

Cite this: *Nanoscale*, 2011, **3**, 3967

www.rsc.org/nanoscale

REVIEW

Li ion battery materials with core–shell nanostructures

Liwei Su, Yu Jing and Zhen Zhou*

Received 30th May 2011, Accepted 27th July 2011
DOI: 10.1039/c1nr10550g

Nanomaterials have some disadvantages in application as Li ion battery materials, such as low density, poor electronic conductivity and high risk of surface side reactions. In recent years, materials with core–shell nanostructures, which was initially a common concept in semiconductors, have been introduced to the field of Li ion batteries in order to overcome the disadvantages of nanomaterials, and increase their general performances in Li ion batteries. Many efforts have been made to exploit core–shell Li ion battery materials, including cathode materials, such as lithium transition metal oxides with varied core and shell compositions, and lithium transition metal phosphates with carbon shells; and anode materials, such as metals, alloys, Si and transition metal oxides with carbon shells. More recently, graphene has also been proposed as a shell material. All these core–shell nanostructured materials presented enhanced electrochemical capacity and cyclic stability. In this review, we summarize the preparation, electrochemical performances, and structural stability of core–shell nanostructured materials for lithium ion batteries, and we also discuss the problems and prospects of this kind of materials.

1. Introduction

The exhaustion of traditional energy and the deterioration of environment have been seriously hindering social development and daily life, especially transportation. Exploring more efficient and environmentally-friendly power devices has attracted tremendous attention in the recent 50 years. Among various devices, lithium ion batteries (LIBs) have been considered the most promising one, in terms of high voltage, large specific capacity, and environmental friendliness.[1] Accordingly, LIBs are being extensively applied in growing diversities from laptops to hybrid electric vehicles (HEVs) and electric vehicles (EVs). However, the current LIB technology cannot satisfy the ever-growing demand for high-performance power sources, and many researchers have been exploring advanced materials including cathodes, anodes, and electrolytes to pursue higher energy and

Institute of New Energy Material Chemistry, Key Laboratory of Advanced Energy Materials Chemistry (Ministry of Education), Nankai University, Tianjin, 300071, China. E-mail: zhouzhen@nankai.edu.cn

Liwei Su

Liwei Su was born in Hebei, P. R. China in 1984. He earned his bachelor's degree in Heibei Technical University, P. R. China (materials chemistry, in 2007) and received his master's degree at Nankai University, P. R. China (materials physics and chemistry, in 2010). Now he is pursuing his Ph D in Nankai University, majoring in inorganic chemistry and working with Prof. Zhen Zhou. Now his research interest mainly focuses on exploring advanced active materials and modification strategies for energy storage and conversion.

Yu Jing

Yu Jing was born in Jiamusi, Heilongjiang Province, P. R. China in 1988. She has recently received her bachelor's degree at Nankai University, P. R. China (June, 2011) majoring in materials chemistry, and then she is going to study for her master's degree at Nankai University, P. R. China with Prof. Zhen Zhou. Her research interest mainly focuses on the synthesis and characterization of transition metal oxides as Li ion battery materials.

power density, longer life, and lower cost. For cathode materials, lots of efforts are focusing on layered $LiMO_2$, olivine-type $LiMPO_4$, and spinel-type LiM_2O_4, where M is one or more transition metal elements.[2–4] Meanwhile, Si, Sn, alloys, and M_nX_m-type compounds (where M = Fe, Co, Ni, Cu, Sn, *etc.*, while X = O, S, N, *etc.*) are investigated as anode materials.[5–7] Though all these active materials show considerable capability and promising prospects, many obstacles restrict their commercialization, including poor electronic conductivity, low Li^+ transfer efficiency, volume expansion/contraction during repeated cycling processes, and loss of active materials due to the corrosion of electrolytes or/and collapse of the stable structure. To overcome these troublesome obstacles, researchers have proposed various feasible strategies, such as optimizing the crystalline lattice of active materials by doping cations or anions, reducing particles to a suitable scale to offer enhanced electron/Li^+ conductivity and reactivity, combining active materials and other active/inactive materials together for complementary strengthening, especially core–shell structures.

Core–shell structures refer to inner cores surrounded by other materials as shells, which source from a traditional concept of the semiconductor field. Generally, the core is the major component with functional properties, while the outer shell acts as a protection layer to strengthen the core performances or to bring new properties. Core–shell composites can also be assembled into zero–three dimensional (0–3D) morphologies in the nanometre to micrometre scale. In this review, core–shell structures and simple mixtures are symbolized with "@" and "/", respectively.

Core–shell structures often exhibit superior physical and chemical properties over their single-component counterparts, and hence are extensively used in optics, magnetism, biomedicine, catalysis, energy conversion and storage, *etc.*[8–17] Since the pioneering work by Liz-Marzán and Mulvaney in 1996,[18] silica-coated nanoparticles have become increasingly important and promising in catalysis and magnetism applications.[19–23] As a typical example, silica-coated metal nanoparticles have been intensively investigated for years. Herein, the metal core can be replaced by metal oxides, polymer templates, or semiconductor nanocrystals, *etc.* Meanwhile, the silica shell can also be substituted with ZrO_2, polymers, other semiconductors as well as carbon materials. Caruso's group has been making great efforts to investigate core–shell structures with different components and has reviewed various preparation methods.[10,11] All the enhanced properties are contributed to the advantages that exterior shells can: 1) protect the core from outside environmental changes; 2) strengthen or bring new physical or chemical properties; 3) restrict volume expansion and maintain the structural integrity; 4) selectively percolate ions or molecules onto the core ; 5) prevent the core from aggregating into large particles, *etc.* (Fig. 1). The exciting advantages of core–shell structures have also been introduced into LIB materials with more and more attention.

In view of the existing obstacles of cathodes/anodes in LIBs, core–shell structures provide a prospective solution. The poor electronic transport and large volume swing during lithiation/delithiation processes are two key problems in newly-proposed cathode and anode materials, and seriously restrict their practical applications. Carbon materials possess both high electronic conductivity and considerable flexibility together; moreover, easy processing and low cost make them attractive for practical applications. Therefore, carbon materials are considered the best coating candidate for the new LIB active materials. Almost all types of LIB active materials have ever been decorated with carbon materials and showed obviously enhanced performances. For the same reason, conducting polymers, transition metals, and inactive metal oxides with high electronic conductivity were also involved to modify the active materials. For some M_nX_m-type anode materials and lithium transition metal oxide (LTMO) cathode materials, however, it is very difficult to avoid the reduction of high-valence metals during thermal treatment at high temperatures.[72] Due to the smaller volume variation of cathodes (1–10%, Table 1),[24,26,37,40,73,74] the carbon shell can be replaced by a thin layer consisting of inactive metal oxides, fluorides, or phosphates. These protection layers can act as HF scavengers to react with the released HF from the electrolyte prior to the active core. Moreover, graphene nanosheets (GNSs) possess high electronic conductivity, large surface areas, open porous structures, flexibility, and chemical stability, and hence have been popular and promising materials in LIBs.[75,76] Very recently, lots of graphene-encapsulated materials have been successfully prepared through different methods and presented exciting performances.

Zhen Zhou

Zhen Zhou was born in Shandong, P. R. China in 1971. After receiving his BSc (applied chemistry, in 1994) and Ph D (inorganic chemistry, in 1999) at Nankai University, P. R. China, he joined the faculty in 1999. Two years later, he began to work in Nagoya University, Japan as a postdoctoral fellow, under the support of JSPS and VBL. In 2005, he returned to Nankai University as an associate professor, and in 2011, he was promoted as a full professor. So far, he has published over 120 papers, 9 patents, and 4 book chapters. His main research interest is material design for energy storage and conversion.

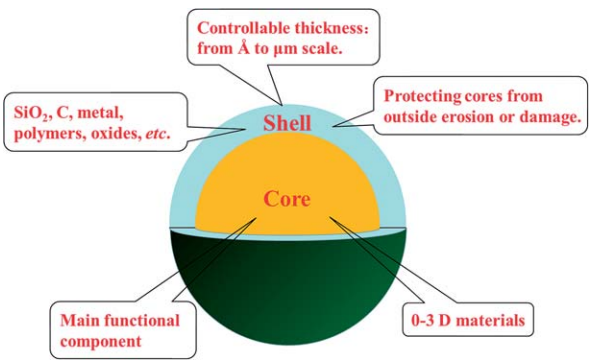

Fig. 1 Schematic representation of typical core-shell structures.

Table 1 Electrochemical properties of main active and coating materials.[a,c]

	Crystal Structure	Limiting Composition	Theoretical Capacity (mAh g^{-1})	Volume Strain $\Delta v/v$	σ (S cm^{-1})	D_{Li^+} (cm^2 s^{-1})	Refs
$LiCoO_2$	α-$NaFeO_2$	$Li_{0.5}CoO_2$	274[b]	1.9%	$\sim10^{-3}$	10^{-9}–10^{-8}	24,25
$LiNiO_2$	α-$NaFeO_2$	$Li_{0.5}NiO_2$	275[b]	2.8%	10^{-1}	10^{-7}	26
$LiMnO_2$	orthorhombic monoclinic	$Li_{0.5}MnO_2$	285[b]	5.6%	10^{-4}–10^{-5}	10^{-16}–10^{-14}	27–31
$LiMn_2O_4$	spinel	Mn_2O_4	148	7.3%	10^{-5}–10^{-3}	10^{-11}–10^{-9}	26,32
$Li_4Ti_5O_{12}$	spinel	$Li_7Ti_5O_{12}$	175	0	10^{-13}	2×10^{-8}	33–35
$LiFePO_4$	olivine	$FePO_4$	170	$\sim$6.8%	10^{-10}–10^{-7}	10^{-15}	36–41
$LiMnPO_4$	olivine	$MnPO_4$	171	9.9%–11%	$<10^{-10}$	10^{-7}	41–46
$LiCoPO_4$	olivine	$CoPO_4$	167	7%	10^{-9}	10^{-9}	42,46–48
$Li_3V_2(PO_4)_3$	NASICON monocilic	$V_2(PO_4)_3$	197	7.4%	10^{-8}–10^{-7}	10^{-8}–10^{-7}	49–51
Si	diamond cubic	$Li_{4.4}Si$	4200	>300%	1.56×10^{-5}[d]	10^{-13}	52–55
Sn	tetragonal	$Li_{4.4}Sn$	994	260%	9.17×10^4	10^{-8}–10^{-7}	26,56
Fe_3O_4	spinel	$Fe^0 + Li_2O$	928	80.3%	10^2	—	53,57,58
SnO_2	rutile	$Li_{4.4}Sn$	783	—	10^{-3}	—	59
TiO_2	anatase rutile	$Li_{0.5}TiO_2$	168	<4%	10^{-10}	10^{-6}[e] 10^{-17}–10^{-10}[e]	35,60–62
graphite	layered	LiC_6	372	13.1%	10^3	10^{-11}–10^{-10}	26,53,63–65
amorphous C	—	—	—	—	10^{-2}–10	—	66
RuO_2	rutile	$Ru^0 + Li_2O$	806	—	10^4	—	67–70
Cu	—	—	—	—	5.96×10^5	—	65
graphene	layered	LiC_3	744	—	10^6	10^{-6}	64,71

[a] All the values were obtained at room temperature. [b] The theoretical capacities of $LiMO_2$ (M = Co, Ni, Mn) are based on the complete extraction of Li ion, while the values of other materials correspond to the conversion from the original phase to the counterpart limiting composition. [c] "–" means that this value is not reported or not significant. [d] The resistivity of semiconductors depends strongly on the presence of impurities in the material. [e] The values were tested in *c*- and *a*-direction of crystalline TiO_2, respectively.

Also, various methods were developed to fabricate LIB materials with core–shell structures during the last 20 years. The initial strategy was mixing as-prepared active materials with carbon materials such as graphite,[77,78] acetylene black,[79,80] and mesocarbon microbead (MCMB)[81] by mechanical milling. Although the electronic conductivity was enhanced to a great extent, and it was applicable in large-scale industrial operations, such rough mixing could not offer enough expansion accommodation in volume and protection from the outside erosion. Replacing the mature carbon materials with a solution of polysaccharides and subsequent carbonization at high temperatures can improve the coating quality. Sol–gel chemistry also attracts tremendous interest as a feasible way to obtain effective coating layers and uniformly distributed particles at the same time.[82,83] Hydrothermal or solvothermal treatments possess particular conditions of high temperature and pressure and are extensively used to prepare regular particles on the nanometre to micrometre scale.[84–86] Also, this route displays advantages to realize advanced core–shell structures, given that polysaccharides can decompose into carbonaceous materials in the high-temperature solution and simultaneously surround the active cores. Other methods include chemical co-precipitation,[87–89] chemical vapor deposition (CVD),[39,90,91] thermal vapor deposition (TVD),[92] microwave-assisted methods,[93] atomic layer deposition (ALD),[94,95] microemulsion,[96] polymerization restriction,[97] spray-pyrolysis,[98] *etc.*

In this review, we focus on the development of core–shell LIB materials, including cathode materials, such as LTMOs with varied core and shell compositions, and $LiMPO_4$ with carbon shells; and anode materials, such as Si, Sn, alloys, and transition metal oxides with carbon shells. Graphene-coated materials will be presented as an important and separate part. Finally, we will summarize the preparation, electrochemical performance, and structural stability of core–shell materials for LIBs, and discuss the problems and prospects of this kind of materials.

2. Lithium transition metal oxides with varied core and shell compositions

Lithium transition metal oxides are regarded as the most successful commercial cathode materials in LIBs up to now. The strong M–O bonds ensure a stable structure for repeated lithiation/delithiation and offer favorable Li^+ transport paths, while lithium and transition metal atoms provide variable Li^+ ions and electrons, respectively. Nowadays, LTMOs are still the hot materials in either laboratories or industries because of their capability and potential in higher capacity and lower cost, especially when they are extended to Li-rich phases. Among diverse LTMOs, layered $LiCoO_2$, spinel-type $LiMn_2O_4$, and $Li_4Ti_5O_{12}$ are the most promising and typical materials, and hence have been attracting tremendous attention. However, there remains poor electronic and Li^+ conductivity, large volumetric swing as well as continuous dissolution or reduction of metal ions in $LiCoO_2$ and $LiMn_2O_4$ during charge/discharge processes.

Decorating the LTMO surface is a feasible strategy to improve the electronic and Li^+ transport, accommodate or restrict the volume variation, and isolate the active cores from outside environment. Carbon coating is regarded as a general surface decoration due to its high electronic conductivity, environmental friendliness, easy preparation, and low cost. However, carbon-coated $LiMO_2$ cathode materials were less reported because the high-valence metal can be reduced at the H_2 or CO atmosphere released during the carbonization of hydrocarbons.[72] Therefore, many active/inactive materials were introduced to substitute for

the carbon protecting layer, which brought greatly enhanced electrochemical behaviors.

2.1 Lithium transition metal oxides coated with carbon

$LiCoO_2$ possesses the layered α-$NaFeO_2$ structure, consisting of alternating infinite layers of edge-sharing CoO_6 and LiO_6 octahedra, and was successfully commercialized as a LIB cathode material years ago, due to lots of advantages such as high voltage of 4.2 V *versus* Li metal, considerable reversible capacity, and ease of production. Actually, there are still some urgent and troublesome aspects in relation to the poor electronic and Li^+ conductivity, high cost, and especially the surface chemical corrosion during storage or work. Optimizing the bulk layered structure by doping other transition metals to form $LiMO_2$, where M is the mixture of two or more elements of Co, Ni, Mn, and Fe, is significantly beneficial to enhance the inherent electronic and Li^+ conductivity, and more importantly, to reduce the production cost. Decreasing the particle size to the nanoscale can also make a positive effect on better electronic and Li^+ transport. However, these alone are insufficient to satisfy the high-rate capability for EVs. To complement the above two strategies, a new surface modification is needed to offer higher electronic conductivity, restrict the expansion in volume, and protect the active materials from outside erosion to a great extent.[24,39,99,100]

Cushing and Goodenough prepared $LiNi_{1/2}Mn_{1/2}O_2$ coated with 2.5 wt% carbon,[99] by combining as-prepared $LiNi_{1/2}Mn_{1/2}O_2$ and resorcinol–formaldehyde polymer or xerogel and subsequently annealing at 600 °C for 6 h in air. More carbon contents could be achieved when heat-treating was performed under an argon atmosphere, and simultaneously Mn^{4+} was reduced to Mn^{3+}. Also, carbon-coated $LiNi_{1/3}Co_{1/3}Mn_{1/3}O_2$ was synthesized by Marcinek and coworkers through a microwave plasma CVD method.[39] This rapid pyrolysis of anthracene precursor took only 2 s and produced an ~10–20 nm thick and sp^2-coordinated carbon layer (0.8–1.2 wt%) on $LiNi_{1/3}Co_{1/3}Mn_{1/3}O_2$ particles. Most recently, porous α-$LiFeO_2$–C nanocomposites with large surface areas and high carbon contents up to 19 wt% have been successfully produced through a molten salt method at a low temperature of 300 °C.[100] The composites with carbon layers delivered a higher reversible capacity and very stable cycle life compared with pure α-$LiFeO_2$. Through the above reports, it is believed that carbon-coated $LiMO_2$ cathode materials can be realized by controlling the atmosphere, pyrolysis time, and heating temperature during the carbonization process, or by exploring other techniques to avoid or restrict the reduction atmosphere.

Spinel-type $LiMn_2O_4$ materials, where Mn can be substituted partially by Ni and Al,[101,102] have long been studied as LIB cathode materials because of their reliable safety and low cost. Besides similar disadvantages of layered $LiMO_2$, $LiMn_2O_4$ shows poor cycling performance at high temperatures (40–60 °C). Similar to pure $LiCoO_2$, it is difficult to modify $LiMn_2O_4$ particles with carbon materials. More studies focus on modifying the surface with inactive metal oxides,[103–105] fluorides,[106] or other materials[107] which can effectively prevent or restrict the active core from the outside erosion.

$Li_4Ti_5O_{12}$ (LTO) with the same spinel-type structure can be used as an anode material of LIBs. When cycling in the voltage window of 1.0–3.0 V, LTO exhibits little structural change and excellent lithiation/delithiation reversibility. As a result, LTO is considered as the most promising anode material for hybrid electrochemical supercapacitors and high-power-density LIBs. However, the high-rate capability is still seriously limited by its inherent insulating nature. In comparison with the instability of layered $LiMO_2$ materials under a reducing atmosphere, carbon-coated LTO composites can be easily obtained, and therefore have been widely investigated to complement its insulating nature. Cheng *et al.* prepared carbon-coated LTO through a TVD process at 800 °C.[108] The graphitized carbon layer of only 5 nm thickness gave a much higher electronic conductivity (2.05 S cm^{-1}) than the raw LTO (10^{-13} S cm^{-1}) and much better rate capability. Moreover, the relatively complete core–shell structure showed superior performance over the rough coating (Fig. 2) for better electronic conductive path and subsequent enough effective reaction areas. It is worth reminding that the graphitized carbon layer is percolated and allows Li^+ ions to transfer from the electrolyte to the inner core.

Reducing LTO particles from the micrometre to the nanometre nanoscale is also an effective way to improve the performance for LIBs.[109–113] Wang *et al.* considered both the "conductive surface modification" and "nano-size" together and developed a method to synthesize LTO@C core–shell composites, in which a typical "nano-size" and "double surface modification based on Ti(III) and carbon" can be achieved simultaneously.[114] In this method, the polyaniline (PANI)-coated TiO_2 particles and a lithium salt were adopted as precursors. On heat treatment under argon atmosphere containing 5% H_2, the carbonization of PANI effectively restricted the particle-size growth of LTO and reduced the surface Ti(IV) into Ti(III). The surface modification combined with tailored particle size can improve the surface electronic conductivity and shorten the Li^+ diffusion path. Moreover, carbon-coated nanostructured LTOs with various morphologies such as nanorods, hollow spheres, and nanoparticles were prepared *via* a simple carbon pre-coating process. In this process, TiO_2 precursors were first coated with a conductive carbon layer by CVD and followed by a solid-state reaction with lithium salt.[90] The surface modification of LTO can also cooperate with doping heavy metals to increase the tap

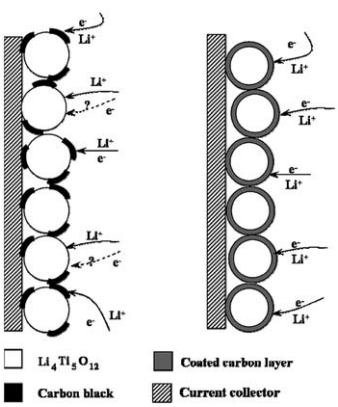

Fig. 2 A schematic representation of the electrochemical reaction path on carbon-mixed (left) and carbon-coated (right) LTO electrodes. (Taken from ref. 108. Reproduced by permission of the Electrochemical Society).

density[115] or replacing the carbon layer with metals[116] and other materials[117] with high electronic conductivity.

2.2 Lithium transition metal oxides coated with other materials

The traditional electrolyte mainly consists of a mixed solvent of cyclic and linear carbonic esters, and the dominated lithium salt of $LiPF_6$, which is sensitive to moisture. In fact, $LiPF_6$-based electrolytes always contain a small amount of water, which greatly propagates the decomposition of $LiPF_6$ salt at elevated temperatures and consequently causes breakdown of the electrolyte, accompanied by HF generation.[118] There are two serious problems which restrict the practical application of active materials. First, the solvent molecules on active materials can decompose into inorganic molecules (such as HF, Li_2CO_3, LiF, LiOH, and Li_2O) and organic molecules (such as $(CH_2OCO_2Li)_2$, $LiCH_2CH_2OCO_2Li$, and CH_3OCO_2Li),[119] and subsequently intercalate into the active materials with Li^+.[120] Second, the active material can first react with HF, and meanwhile the solvent can be oxidized by the high-valence metals in active materials to form a stable and double-headed solid electrolyte interface (SEI) film. These side reactions induce a great loss of charge capacity (the schematic mechanism is shown in Fig. 3).[121] Lots of efforts have been made to avoid the loss of active materials and direct contact between the active material and electrolyte during repeated lithiation/delithiation processes. An ongoing and promising solution is to exploit suitable additives for the electrolyte, which can preferentially produce an effective SEI film. However, few ideal candidates are found for cathode materials. Another feasible solution is to modify the surface with inactive materials, which can isolate the contact with the electrolyte, react with HF, and simultaneously form a protection layer against further erosion and co-intercalation of the solvent molecules.

Additionally, the dense inactive layer should stabilize the crystalline lattice and hence enhance the cyclic stability. Among them, inactive metal oxides were earlier adopted to coat $LiCoO_2$ particles by Cho *et al.*[123–126] They considered that the high concentration of surface metal atoms can effectively suppress the lattice-constant changes during electrochemical cycling and thereby avoid the unwanted phase transition, and further demonstrated that the larger fracture toughness had better cycling behaviors in the order $ZrO_2 > Al_2O_3 > TiO_2 > B_2O_3$, and ZrO_2 layers offered the best capacity retention. However, they did not discover the nanocrystalline ZrO_2 layer coating on the particles and instead, assumed that ZrO_2 reacted with $LiCoO_2$ and formed a previously unreported $LiZr_xCo_{1-x}O_2$ phase, which was beneficial to avoid the lattice expansion and contraction during insertion/extraction processes. On the contrary, Chen *et al.* confirmed the existence of the ZrO_2 coating layer by means of *in situ* X-ray diffraction (XRD), and proved that the coating layer did not affect the lattice expansion of $LiCoO_2$.[127] The improved performance may be attributed to the reduced contacting area between $LiCoO_2$ and the electrolyte. Similarly, Liu *et al.* confirmed the structure of the Al_2O_3 coating on $LiCoO_2$ with *in situ* XRD and considered that, in order to improve the capacity retention, one should try to preserve the variation range of the lattice parameters, not suppress it.[128] In the past ten years, cathode materials coated with various oxides, including Al_2O_3,[129,130] ZrO_2,[129–132] ZnO,[103,133,134] SiO_2,[129] TiO_2,[130,135] Cr_2O_3,[104] SnO_2,[123] Li_2O–B_2O_3 glass,[107] and high–conductivity CeO_2,[105,136] have been fabricated and showed better electrochemical behaviors even at high temperature and high potential.

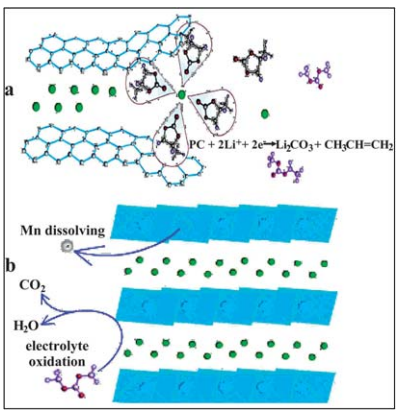

Fig. 3 (a) Decomposition and co-intercalation of solvent molecules on anode electrodes and (b) dissolution of cathode material and decomposition of solvents. (Taken from ref. 122. Reproduced by permission of Editorial Office of Progress in Chemistry).

Thus, what is the real modification mechanism of oxide coating layers? In 2005, Myung *et al.* investigated the interface reaction between the Al_2O_3-coated $Li[Li_{0.05}Ni_{0.4}Co_{0.15}Mn_{0.4}]O_2$ and liquid electrolyte, and put forward a new mechanism against the physical protection. They considered that Al_2O_3 can react with the released HF from electrolytes and form the byproduct of AlF_3, which can be confirmed by examining the cycled active materials through a time-of-flight-secondary ion mass spectroscopy (ToF-SIMS).[118,137] Based on the existence of Al–O–F and Al–F fragments detected by ToF-SIMS, they assumed that the formation of Al–O–F would be in an intermediate stage to be transformed to Al–F bonds which scavenges F^- from HF, and further speculated the reaction mechanism as below:

$$Al_2O_3 + 2HF \rightarrow Al_2O_2F_2 + H_2O \quad (1)$$

$$Al_2O_2F_2 + 2HF \rightarrow Al_2OF_4 + H_2O \quad (2)$$

$$Al_2OF_4 + 2HF \rightarrow 2AlF_3 + H_2O \quad (3)$$

Considering the above results, Sun *et al.* directly prepared AlF_3-coated $LiCoO_2$ and surprisingly discovered that the capacity retention and rate capability were greatly enhanced at a high cut-off voltage of 4.5 V.[138] The improved electrochemical performance could be explained by the reduced Co dissolution and less formation of LiF films which can increase cathode/electrolyte interfacial impedance. Following this exciting result, various cathode materials coated with fluorides, such as AlF_3,[139–143] SrF_2,[144] ZrF_x,[145] and BiOF,[102,106] have been studied in depth and showed better electrochemical performances, especially at elevated temperatures and high cut–off voltages.

As another Al-containing solid-solution layer, $AlPO_4$ can also react with HF and form the "Co–Al–O–F" type of thin film to reduce Co dissolution as well as surface reactions between active particles and electrolytes.[87,146–148] In contrast, the bare "$LiCoO_2$" particles are exposed to and react with the electrolyte,

continuously form highly resistant decomposition products (LiF and $Li_xPF_yO_z$) of the electrolyte, and then isolate the active particle. Co dissolution and oxygen loss also lead to structural instability such as formation of the stacking fault. The proposed mechanism is shown in Fig. 4. Inspired by the stable and robust structure of phosphates, researchers successfully synthesized $Mg_3(PO_4)_2$-coated $Li_{1.05}Ni_{1/3}Mn_{1/3}Co_{1/3}O_2$ and $FePO_4$-coated $LiCoO_2$ cathode materials, which presented improved high-rate capabilities and thermal stability.[88,149] Li *et al.* assumed that the superiority of $FePO_4$-coated $LiCoO_2$ over the bare counterpart may be attributed to the strong P–O bond which was very resistant to chemical attack. The high thermal stability of the $FePO_4$ layer may be attributed to the strong covalence of the PO_4^{3-} polyanions with the Fe^{3+} ions in $FePO_4$.

However, the metal oxide, fluoride, and phosphate layers mentioned above are all inactive materials to Li^+ at a high cut-off voltage; therefore, more coating materials induce less specific capacity. Hu *et al.* compared the electrochemical and thermal performances of $Co_3(PO_4)_2$- and $AlPO_4$-coated $LiNi_{0.8}Co_{0.2}O_2$ cathode materials and demonstrated a different mechanism for improvement.[48,150–152] $Co_3(PO_4)_2$-coated $LiNi_{0.8}Co_{0.2}O_2$ exhibited a higher reversible capacity and better capacity retention because of the lithium-reactive $Co_3(PO_4)_2$ coating. This $Co_3(PO_4)_2$ layer could react with LiOH and Li_2CO_3 impurities during annealing and form an electrochemically and thermally stable Li_xCoPO_4 shell. Logically, $LiFePO_4$ can be adopted to modify the surface of active particles for its high specific capacity and good cyclic stability even at high temperatures and high potentials.[153–155]

2.3 Two promising core–shell LTMOs

To maximize the Li-storage capability of LTMOs, two promising core–shell strategies were proposed, concentration-gradient outer shells or an ultrathin Al_2O_3 coating, demonstrating significant electrochemical performance improvements.

Combining the better electrochemical behavior of the core material and lower reactivity of the shell material may be an effective strategy for LIB cathode materials.[72] Following this line, Sun's group made a significant breakthrough in the development of cathode materials with two typical core–shell structures. One is the core–shell $Li[(Ni_{0.8}Co_{0.1}Mn_{0.1})_{0.8}(Ni_{0.5}Mn_{0.5})_{0.2}]O_2$ active material, in which the inner core part possesses a high capacity and the counterpart shell provides thermal stability.[89,157] The core Li $[Ni_{0.8}Co_{0.1}Mn_{0.1}]O_2$ was believed to undergo a volume change of approximately 9–10%,[158] whereas the shell $Li[Ni_{0.5}Mn_{0.5}]O_2$ volume change was only 2–3% during lithiation/delithiation processes.[159] This discontinuity results in a drastic decline in battery performance.[156] To complement this shortcoming, Sun *et al.* put forward another typical core–shell structure of Li $[Ni_{0.68}Co_{0.18}Mn_{0.18}]O_2$, in which each particle consists of bulk material surrounded by a concentration-gradient outer layer. As illustrated in Fig. 5, the bulk is a nickel-rich layered oxide $(Li[Ni_{0.8}Co_{0.1}Mn_{0.1}]O_2)$ to satisfy the high energy and power requirement for the EVs. In the outer layer, the reactive nickel ions are gradually replaced with manganese ions to the resulting surface composition of $Li[Ni_{0.46}Co_{0.23}Mn_{0.31}]O_2$, which is much more stable in contact with the electrolyte than the bulk composition. This material showed not only a very high reversible capacity of 209 mAh g^{-1}, but also excellent cycling and safety characteristics. This novel approach should lead to the design and development of a wide range of safe, stable, and high-capacity materials for advanced LIBs.

Almost all the above coating materials show inherently poor conductivities and Li-storage capabilities. Thus, thicker coating layers lead to worse electronic transport and less specific capacities. Also, the volume variation of $LiCoO_2$ during cycling is only 1.9%,[26] and hence is not necessary to be accommodated. Therefore, a complete coating layer with a suitable thinness is more beneficial for both the specific capacity and high-rate performance. Recently, Scott and coworkers have made a breakthrough in controlled full-electrode nanoscale coatings that enabled nanomaterials to cycle with durable high energy and remarkable rate performance.[94] They successfully realized ultrathin Al_2O_3 coatings on nano-$LiCoO_2$ cathode materials through atomic layer deposition (ALD), which is a well established method to apply conformal thin films with controlled thickness at the atomic level on High-surface area tortuous networks through sequential, self-limiting surface reactions.[95,160] Different from the simple physical coating on active particles, Al_2O_3 ALD layers can directly grow on the nano-$LiCoO_2$ particles to form a dense and tight film (Fig. 6) and hence suppress undesirable side reactions and thereby act as a stable "artificial" SEI film that can quickly transport Li^+ ions and widen the voltage window. The Al_2O_3 (~1–2 nm thickness) coated

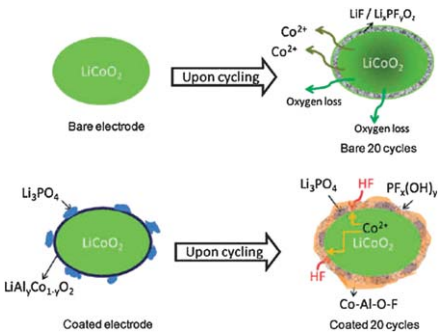

Fig. 4 Proposed working mechanism of "$AlPO_4$"-coated $LiCoO_2$. (Taken from ref. 146. Reproduced by permission of the American Chemical Society).

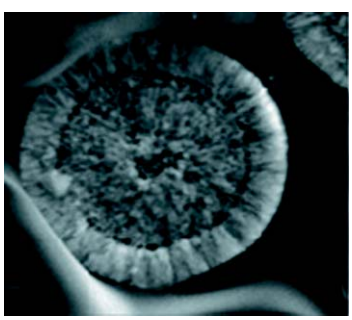

Fig. 5 A SEM image of a cathode particle with a Ni-rich core surrounded by a concentration-gradient outer layer. (Taken from ref. 156. Reproduced by permission of Nature Publishing House).

nano–$LiCoO_2$ electrodes delivered a discharge capacity of 133 mAh g^{-1} at a high current of 1400 mA g^{-1} (7.8 C), corresponding to a 250% improvement in reversible capacity compared with bare nanoparticles. These amazing results for Al_2O_3 ALD-coated $LiCoO_2$ powders may lead to opportunities for nanomaterials to be used in commercial LIBs.

3. Phosphates with carbon shells

Since the proposal of $LiFePO_4$ by Goodenough *et al.* in 1997, olivine-type $LiMPO_4$ (where M = Fe, Mn, Co, or Ni) materials have been extensively studied as promising cathode materials in LIBs, in terms of high charge/discharge voltage, large specific capacity, suitable thermal stability, and low toxicity. $LiFePO_4$ is particularly attractive due to their abundant and cheap raw materials. Vanadium-based phosphate cathode materials including $Li_3V_2(PO_4)_3$, $LiVOPO_4$, and $LiVPO_4F$ are also attracting tremendous attention, given that the rigid phosphate network offers good electrochemical and thermal stability. Similarly, poor electronic and ionic conductivity seriously hamper their practical applications. Optimizing the crystalline lattice by doping transition metals or polyanions is regarded as an effective way to improve the inherently electronic and Li^+ ion conductivity.[161] However, this alone is not enough to meet the high-rate requirement for EVs. More efforts have been focusing on modifying the surface with high-conductivity carbon layers.

3.1 $LiFePO_4$ with carbon shells

In 1999, Ravet *et al.* reported that $LiFePO_4$ had a capacity of about 160 mAh g^{-1} at 1 C rate at 80 °C when coated with about 1 wt% carbon. This indicated that increasing the conductivity can improve the capacity significantly. After this report, various techniques were developed to realize the carbon-coated $LiFePO_4$ particles on the micrometre to nanometre scale. Mechanically mixing as-prepared $LiFePO_4$ powders with high electrically-conductive carbon materials such as graphite, MCMB, and acetylene black can obtain a rough-coating structure, in which active particles are not completely coated with the carbon layer and lots of bare areas are exposed to air or electrolytes.

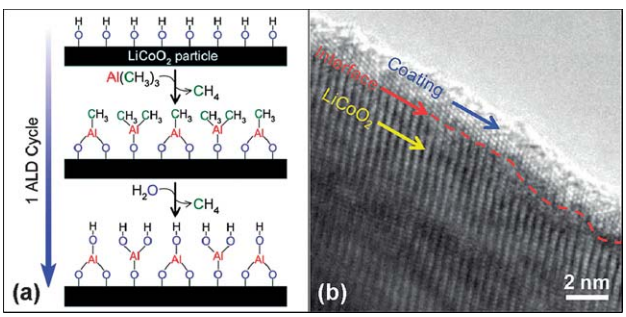

Fig. 6 (a) A schematic representation of Al_2O_3 ALD on $LiCoO_2$ powder. (Taken from ref. 160. Reproduced by permission of the Electrochemical Society). (b) A High-Resolution Transmission Electron microscopy (HRTEM) image of Al_2O_3-coated nanosized $LiCoO_2$ particles by 6 ALD cycles on the bare powder. (Taken from ref. 94. Reproduced by permission of the American Chemical Society).

Although these techniques significantly improved the electronic conductivity, the uncoated areas remain weak sites for the attack of O_2 and non–aqueous electrolytes. An improved method is to adopt polysaccharides[83,162–166] and polymers[97,167–169] as carbon sources carbonized at high temperatures. In solution, polysaccharide or polymer molecules can satisfactorily adhere to the surface of $LiFePO_4$ particles by coulombic forces or chemical adsorption. Meanwhile, it is easier to obtain evenly distributed nanoparticles in solution than in solid phases. As a typical example, Wang and coworkers reported an *in situ* polymerization restriction method for the synthesis of $LiFePO_4$@carbon nanocomposites with PANI as the carbon source.[97] In a typical synthesis, Fe^{3+} ions were added to a solution containing PO_4^{3-} ions and acted as a precipitator for PO_4^{3-} first, and then a very small amount of surface Fe^{3+} ions of the as-obtained precipitate led to the oxidization polymerization of aniline. The reaction mechanism during this process can be summarized in eqns (4) and (5).

$$Fe^{3+} + PO_4 \rightarrow FePO_4^{3-} \downarrow \quad (4)$$

$$(FePO_4)_{surface}Fe^{3+} + n(\text{Aniline}) \rightarrow (FePO_4)_{core}(\text{Polyaniline})_{shell} \quad (5)$$

The PANI molecules were directly polymerized on the newly produced $FePO_4$ particles with a size of about 20–40 nm to restrict its further growth and subsequently formed a semi-graphitic carbon shell with a thickness of about 1–2 nm after heating at 700 °C. $LiFePO_4$@C composites could be obtained in the presence of Li salts during heat treatment. The prepared composites showed a high capacity of 168 mAh g^{-1} at a current density of 0.1 A g^{-1} (~0.6 C rate) and an excellent cycling performance, with less than 5% discharge capacity loss over 1100 cycles.

Although it is demonstrated that the poor electronic conductivity can be improved by perfect carbon coating as mentioned above, the high cost and low tap density of nanomaterials always hamper their practical application to a great extent. Recently, Oh *et al.* have adopted sucrose as a carbon source to prepare carbon-coated $LiFePO_4$ with a 6 μm spherical particle size, which delivered a tap density of 1.5 g cm^{-3}, and excellent electrochemical performance.[164,170] This material was composed of carbon-coated micrometre-scale secondary particles containing nanoscale carbon-coated primary particles; such morphology provided interconnected open pores that favor electrolyte absorption and significantly reduce the diffusion path of lithium ions. Following this line, they further fabricated double carbon-coated (DCC) $LiFePO_4$ and greatly improved the uniformity of the carbon coating on both the primary and secondary $LiFePO_4$ particles (Fig. 7). In coin-type cell tests, the electrodes composed of this material presented superior specific capacities, rate capabilities, and volumetric energy densities. This DCC structure may give enlightenment on practical utilization of nanomaterials.

3.2 $LiMnPO_4$ and $LiCoPO_4$ with carbon shells

$LiMnPO_4$ and $LiCoPO_4$ show higher potentials (4.1 V and 4.8 V *vs.* Li^+/Li, respectively) than $LiFePO_4$ (3.4 V *vs.* Li^+/Li). Also, many efforts have been made on the surface modification with

carbon.[171–176] Murugan *et al.* synthesized carbon-coated $LiMPO_4$ (M = Fe, Mn, Co) materials *via* one-pot microwave-hydrothermal *in situ* carbonization of glucose.[171] Although the $LiFePO_4$@C nanocomposites exhibited high capacities with excellent cyclic stability and rate capabilities, both $LiMnPO_4$@C and $LiCoPO_4$@C showed inferior reversible capacities of only 22 and 52 mAh g^{-1}, respectively, which can be ascribed to the low electronic conductivity of $LiMnPO_4$ and the lack of stable electrolytes at the high operation voltage of 4.8 V for $LiCoPO_4$.

Oh *et al.* synthesized carbon–$LiMnPO_4$ nanocomposites by ultrasonic spray-pyrolysis followed by ball milling, delivering a discharge capacity of 158 mAh g^{-1} at 0.05 C, 126 mAh g^{-1} at 1 C, and 107 mAh g^{-1} at 2 C rate, which are the highest capacities reported so far for this type of material.[173] The improved performances referred to the homogeneous coating of the acetylene black, which can protect $LiMnPO_4$ against HF attack and simultaneously lead to significantly less Mn dissolution, lower charge-transfer resistance, and better electronic conductivity.

In contrast, it is difficult to modify the $LiCoPO_4$ surface with carbon materials.[176] Li *et al.* developed a simple and rapid method to synthesize $LiCoPO_4$@C nanocomposites *via* microwave heating.[93] The discharge capacity of $LiCoPO_4$@C was maintained 72.6 mAh g^{-1} after 30 cycles at a current rate of 0.1 C, much higher than pure $LiCoPO_4$. The carbon-coating film not only increased the electrical conductivity, but also prevented the direct reactions between high-valence Co and electrolytes.

3.3 $Li_3V_2(PO_4)_3$ with carbon shells

$Li_3V_2(PO_4)_3$ has two different frameworks: rhombohedral (NASICON) and monoclinic phase, containing three independent lithium sites with a theoretical discharge capacity of 197 mAh g^{-1}, while three Li ions are completely extracted up to 4.8 V. However, $Li_3V_2(PO_4)_3$ has poor electronic conductivity similar to $LiFePO_4$. This problem can be solved to some degree by doping metals or mixing with electrically conductive materials such as carbon. In 2002, Huang and coworkers prepared nanostructured $Li_3V_2(PO_4)_3$/C composites, in which carbon came from the polymerization of resorcinol–formaldehyde (RF) sol to a carbon gel and subsequent heating treatment.[177] The existence of the RF sol restricted the particle size and instead formed densely packed agglomerates. The $Li_3V_2(PO_4)_3$ crystallites were of above 50 nm on average with a thin carbon wall sponge of ~100 nm in thickness. The homogenously dispersed $Li_3V_2(PO_4)_3$ nanocrystallites in the carbon matrix presented excellent performances. When cycling at 0.2 C in the voltage window of 3.0–4.3 V, a reversible capacity of 132 mAh g^{-1} was achieved corresponding to two Li's per unit completely extracted from $Li_3V_2(PO_4)_3$. Even at the rate of 5 C, 95% theoretical capacity still remained.

In addition, Ren *et al.* synthesized the monoclinic $Li_3V_2(PO_4)_3$@C with a typical core–shell structure through a sol–gel route and a subsequent hydrothermal procedure.[82] The $Li_3V_2(PO_4)_3$ particles encapsulated with an amorphous carbon shell of ~10 nm in thickness (see Fig. 8a). After 50 cycles at 0.2 C in the voltage window of 3.0–4.5 V, the core–shell composites still displayed a high capacity of 125.9 mAh g^{-1} (see Fig. 8b), which is close to the theoretical value. Moreover, combining the core–shell structure and metal dopants or exploiting more suitable carbon sources can further improve the electrochemical performances.[178–181]

Up to now, almost all the reported $Li_3V_2(PO_4)_3$ materials work at the voltages below 4.5 V due to its instability in traditional electrolytes. Practical utilization of the full capacity under prolonged cycling conditions will reply on electrolytes stable at high potentials.[178] Core–shell structures should also play an indispensable role in improving the high-voltage performances of the above materials.

4. Si, Sn, and alloys with carbon shells

Compared with cathode materials, anode materials have even more severe problems, not only low electronic conductivity and Li^+ diffusion, but also large volume expansion/contraction. As a typical example, Si-based materials have received tremendous interest for their extremely high theoretical capacities of approximately 4200 mAh g^{-1} (corresponding to the formation of $Li_{4.4}Si$ alloy), which is 11 times that of the commercialized graphite (372 mAh g^{-1} for LiC_6). However, the dramatic volume swing (up to 400%) during alloy/dealloy processes leads to the pulverization of the electrode materials and breakdown of the electrically conductive network, and hence restricts the practical

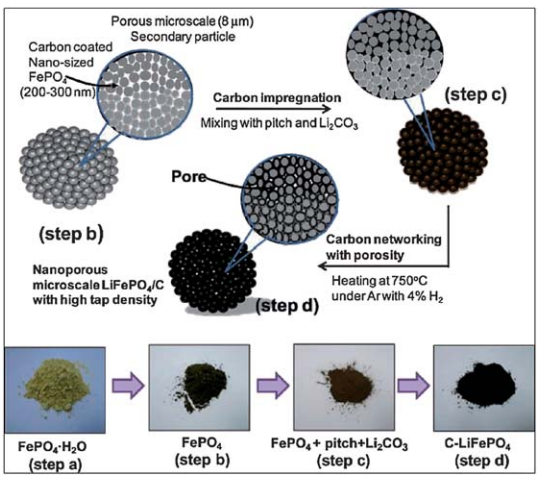

Fig. 7 A schematic representation of the formation procedure and photographs of spherical microscale nanoporous $LiFePO_4$/C composites. (Taken from ref. 164. Reproduced by permission of John Wiley and Sons).

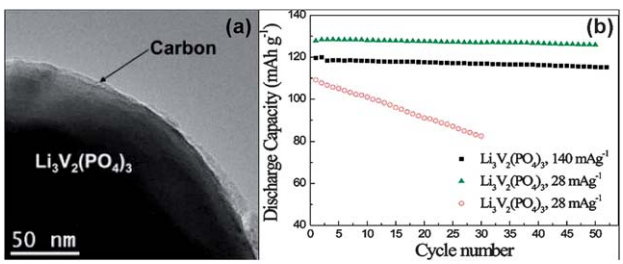

Fig. 8 A TEM image of $Li_3V_2(PO_4)_3$@C composite (a) and cyclic performances of $Li_3V_2(PO_4)_3$ and $Li_3V_2(PO_4)_3$@C tested at different current densities at 25 °C (b). (Taken from ref. 82. Reproduced by permission of the American Chemical Society).

application seriously.[182,183] Moreover, Sn- and Sb-based materials are also attracting more and more attention for high capacities of 994 mAh g^{-1} (for $Li_{4.4}Sn$) and 660 mAh g^{-1} (for Li_3Sb), small volume change and good electronic transport. To improve their performances, most studies focus on three strategies: reducing particle size to nanoscale, changing more effective binders, and adopting composite materials, especially with core–shell structures.

4.1 Si nanoparticles with carbon shells

Lots of efforts have been made on Si-based composites in which Si is homogenously dispersed in active/inactive matrix to accommodate the strain and maintain the structural integrity. Among various favorable matrixes, carbon materials are the most promising candidates in terms of high electronic conductivity, good elasticity, abundance, easy preparation and hence low cost. For example, roughly C-coated Si composites have been synthesized in various ways, exhibiting relatively stable capacities from 500 to 900 mAh g^{-1}.[54,184–186] In these cases, micro-Si was chosen as the active material since nano-Si is hard to be coated with carbon without any pretreatment due to its large surface stress. Although it is expected that the transformation from bulk to nanostructures results in higher interfacial areas, shorter path lengths for Li^+ transport, and better accommodation of the lithiation/delithiation strain, the active surface of nano-Si powder brings more side reactions as well as higher irreversible capacity. From another viewpoint, the carbon shell can compensate these shortcomings from nanosization in terms of restricting side reactions and aggregation during alloy/dealloy processes. Therefore, to prepare nanostructured Si-based composites coated with a carbon shell is the most promising solution to improve the electronic conductivity and simultaneously overcome the shortcomings from nanosization.

Si@C composites can be obtained by ball-milling Si nanoparticles and carbon; however, such mechanical mixing results in loose and inhomogeneous electrical contact. In order to obtain complete carbon coating, it is necessary to decorate the surface of Si nanoparticles or to exploit novel preparation techniques. In 2006, Ng *et al.* successfully produced carbon-coated Si nanocomposites by a spray-pyrolysis technique, in which nanocrystalline Si powders were homogeneously dispersed into the citric acid/ethanol solution in the weight ratio of 1 : 10 (Si/citric acid), *via* ultrasonication for 90 min. Subsequently the obtained solution was pyrolyzed in a vertical-type spray pyrolysis reactor in air, with a flow rate of 4 mL min^{-1}.[98,187] The as-synthesized Si@C materials can reversibly store lithium with both a high capacity of 1489 mAh g^{-1} and a high coulombic efficiency of over 99.5% even after 20 cycles. The long-time ultrasonication and special pyrolysis style were beneficial for the citric acid coating and *in situ* carbonization on the core particles. Similarly, Gao *et al.* adopted poly(cyclotriphosphazene-4,4-sulfonyldiphenol) (PZS) as the encapsulating polymer with respect to its easy synthesis route, good interface compatibility with the inorganic phase and intrinsic thermosetting property, which is beneficial to avoid conglutination and incorporation of nanoparticles during the pyrolysis process (Fig. 9a).[86] A long-time ultrasonic treatment was also performed during PZS encapsulation, which effectively prevented agglomeration of the high-surface-energy nanoparticles in solvents. The improved cyclability of over 1200 mAh g^{-1} should be attributed to homogeneous distribution of nanosized Si particles in the amorphous carbon matrix.

For Si@C nanocomosites, the binding of Si and C is very critical for the performance enhancement. It is regarded that a SiO_2 layer or covalent linkage can promote the growth of a dense carbon layer on Si particles upon heat treatment. Hu *et al.* realized the preparation of Si@SiO_x/C nanocomposite only through a hydrothermal process.[188] This nanocomposite presented a large reversible capacity of about 1100 mAh g^{-1} up to 50 cycles with the help of vinylene carbonate (VC)-containing electrolytes. More recently, Su *et al.* have proposed core double-shell Si@SiO_2@C nanocomposites by modifying the nano-Si surface with a well-proportioned Li_4SiO_4 layer prior to the carbon coating during a hydrothermal treatment (Fig. 9b).[84] Li metal and pure nano-Si were homogeneously mixed by ball milling with acetone as the lubricant. An Ar atmosphere was adopted to avoid oxidation of Li ahead of schedule. After sintering at 400 °C for 2 h, a well-proportioned Li_4SiO_4 layer formed and was then decomposed into SiO_2, while glucose was carbonized during the hydrothermal process to form the carbon layer. The modification of the Si surface by SiO_2 films was of benefit for the subsequent C-coating, which can be ascribed to hydroxyl groups yielded from hydrolysis of Li_4SiO_4. These reactions can be simply described in eqns (6) and (7):

$$4Li + 2O_2 + Si \rightarrow Li_4SiO_4 \quad (6)$$

$$Li_4SiO_4 + 2H_2O \rightarrow SiO_2 + 4LiOH \quad (7)$$

Besides the above reports, more core–shell Si@C nanocomposites were successfully prepared by dispersing nanocrystalline Si in carbon aerogels and subsequent carbonization, and exhibited reversible capacities of over 1000 mAh g^{-1}.[189]

4.2 Si nanowires and nanotubes with carbon shells

In comparison with Si@C nanoparticles, core–shell Si@C nanowires and nanotubes always show even higher reversible capacities and better high-rate performances, given that carbon coated 1D materials can offer high electronic transport and good accommodation for volume expansion, especially when nanowires/nanotubes directly and regularly grow on the current collector in LIBs.

In 2008, Kim *et al.* reported mesoporous Si@C core–shell nanowires with a diameter of ~6.5 nm.[190] The as-synthesized core–shell Si@C nanowires demonstrated an excellent initial charge capacity of 3163 mAh g^{-1} with a coulombic efficiency of

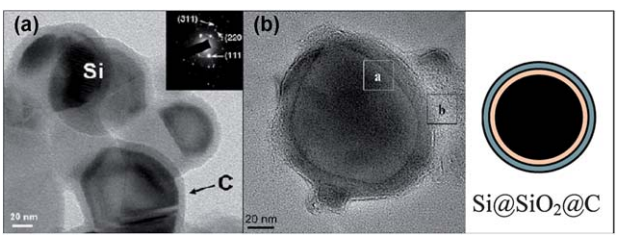

Fig. 9 TEM images of Si@C (a) and Si@SiO_2@C (b). (Taken from refs 86 and 84. Reproduced by permission of the Royal Society of Chemistry).

86% at a rate of 0.2 C (600 mA g^{-1}) between 1.5 and 0 V. Moreover, the capacity retention after 80 cycles was 87%, while the rate capability at 2 C (6000 mA g^{-1}) was 78% of that at 0.2 C. Hertzberg *et al.* fabricated core–shell Si@C nanotubes by using carbon nanotubes (CNTs) with an inner Si layer *via* SiH_4 decomposition at 500 °C.[191] The compressed Si tubes were typically attached to the CNT walls, providing electrical contact. Similar levels of volume contraction in Si inner tubes and no major defects in the carbon walls were observed after cycling, suggesting reversible shape changes. The sample with a Si content of 46 wt% showed a capacity of 2100 mAh g^{-1}.

Even if the high-conductivity carbon was replaced by other materials, core–shell 1D Si materials still showed enhanced electrochemical performances. Cui *et al.* fabricated crystalline–amorphous core–shell Si nanowires grown directly on stainless steel current collectors.[192] Amorphous Si was selected as the shell and crystalline Si as the core, due to the difference in their lithiation potentials. Therefore, crystalline Si cores function as a stable mechanical support and an efficient electrical conducting pathway while amorphous shells store Li^+ ions. Such core–shell nanowires presented a specific capacity of ~1000 mAh g^{-1} and capacity retention of ~90% over 100 cycles.

Although core–shell Si@C composites including Si nanoparticles and 1D nanomaterials showed greatly enhanced specific capacities and high-rate stability, they are still far from practical utilization due to their complicated preparation route, high cost, and low tap density. To design a DCC structure like $LiFePO_4$ mentioned above will be a feasible solution.

4.3 Sn- and Sb-based core-shell materials

With respect to Sn- and Sb-based materials, active nanoparticles can be highly dispersed in active/inactive balls and further coated with another carbon shell (we call it nutty-cake structure), very similar to the DCC structure.[193,194] This structure can offer a considerable tap density, more expansion space, enhanced electronic transport framework, a good isolator layer between the high-activity metal sites and electrolytes, and hence improved energy density and cycling stability. A TEM image of Sn@C and schematic illustration of preparing $Sb/Al_4C_3/C$ with the nutty-cake structure are shown in Fig. 10. Moreover, SiC@Sn@C nanocomposites with a sandwiched structure were also synthesized by Chen *et al.*, which presented a high Li-storage capacity of 600 mAh g^{-1} and a quite high rate capability when used as anodes for LIBs.[195] The rigid SiC nanocores can accommodate the mechanical strain of the lithiated Sn layer produced during the charge/discharge process, and meanwhile the outer carbon shell can not only bind the Sn nanolayer to avoid pulverization and provide good electrical contact among the particles, but also prevent the nanoparticles from aggregating during cycling. Very recently, Kim *et al.* have produced a novel core–shell Sn-based material in which a Cu shell with higher electrical conductivity (6×10^5 S cm^{-1}) was adopted to replace the traditional carbon (1.1×10^2 S cm^{-1}) (see Table 1). Compared with Sn@C nanoparticles, Sn@Cu core–shell nanomaterials showed a greatly enhanced high-rate capability of 620 mAh g^{-1} at 6 C (3.6 A g^{-1}). The highly conductive copper shell played a dominant role in improving the capacity retention.[196]

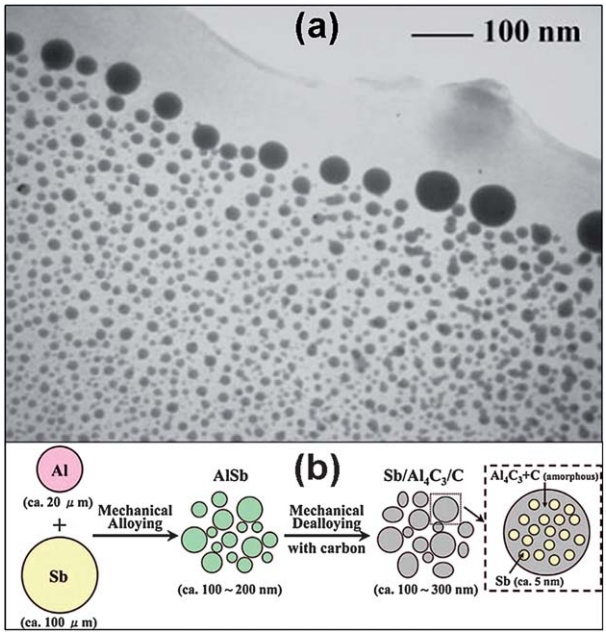

Fig. 10 (a) A TEM image of Sn@C with a nutty-cake structure. (Taken from ref. 193. Reproduced by permission of John Wiley and Sons). (b) A schematic illustration of preparing the $Sb/Al_4C_3/C$ nutty-cake structure. (Taken from ref. 194. Reproduced by permission of the American Chemical Society).

More recently, new effort has been made on exploiting advanced core–shell structures and techniques to improve the electrochemical performance of Sn- and Sb-based materials.[197–199]

5. Metal oxides with carbon shells

Since metal oxides (MOs) were proposed as high-performance anode materials for LIBs by Poizot *et al.* in 2000, more and more researchers have been exploring efficient MO anode materials.[200] Though various MO materials, including Co_3O_4, CoO, Fe_2O_3, Mn_3O_4, MnO, NiO, CuO, SnO, Cr_2O_3, MoO_3, and MoO_2, are attracting great attention, most studies mainly focus on Fe_3O_4, SnO_2 and TiO_2 in terms of good electrochemical capability and especially low lost. The mechanism of Li storage in MO materials differs from the classical Li insertion/deinsertion or Li-alloying/dealloying processes, and involves the formation and decomposition of Li_2O, accompanying the reduction and oxidation of metal nanoparticles. The conversion mechanism can be typically depicted as $M_nO_m + 2mLi^+ + 2me^- \leftrightarrow nM + mLi_2O$, in which M_nO_m excludes SnO_2 and TiO_2. However, the huge volume change during these repeated processes, poor electronic conductivity (except Fe_3O_4) and low coulombic efficiency hamper their practical applications. The combination of nanosization and core–shell structures provides a feasible strategy for performance improvement due to a decreased Li^+ ion transfer distance, buffered volume expansion, and increased electronic conductivity.

5.1 Fe_3O_4 with carbon shells

One of the promising oxide anode materials is magnetite (Fe_3O_4), which has a high theoretical capacity (~928 mAh g^{-1}), low cost,

good stability, environmental friendliness, and especially high electronic conductivity which is very precious among MOs (see Table 1). The biggest problem for Fe_3O_4 is the large expansion during cycling and subsequent pulverization as well as the low initial coulombic efficiency. Carbon coating can play an effective and important role in accommodating the volume change and maintaining the structure integrity.

Sun and coworkers introduced a one-pot hydrothermal treatment to prepare oxide@C core–shell nanostructures with carbonaceous shells and oxides (including hydroxides or complex oxides) cores.[201] Hydrolyzable metal salts are introduced into a clear solution of glucose or other solvable saccharides, and hydrolyze/dehydrate under ambient or hydrothermal conditions to form oxide (or hydroxide, complex oxide) nano- or microparticles (Step I). As-formed carbonaceous materials encapsulate former oxide particles to form a thin sheath (Step II), which is penetrable for small molecules such as amine or hydrazine. The oxide cores could react with the carbonaceous shell or other introduced chemical reagents to convert into core–shell nanostructures (Step III). Besides hydrolyzation, various chemical reactions can be introduced under the aforementioned hydrothermal conditions before the carbonization of saccharides. This significantly enriches the accessible core–shell structured nanoparticles.

Following this line, Wan's group synthesized carbon-coated Fe_3O_4 nanospindles (Fig. 11a) by partial reduction of monodispersed hematite nanospindles with carbon coatings under hydrothermal conditions.[202] The presence of amorphorous carbon layers on the surface of Fe_3O_4 nanospindles reduced the risk of side reactions, restricted the volume variation of the electrode, and avoided the pulverization of the electrode. Also, the carbon layers with high electronic conductivity can act as efficient electrically conductive networks. As a result, the as-obtained Fe_3O_4@C nanocomposites showed high reversible capacities (745 mAh g^{-1} at 0.2 C and 600 mAh g^{-1} at 0.5 C), high coulombic efficiencies in the first cycle, and significantly enhanced cycling performances and high rate capabilities compared with bare hematite spindles and commercial magnetite particles. Similarly, core–shell Fe_3O_4@C nanowires (Fig. 11b) were prepared *via* a microwave-hydrothermal approach assisted with polyethylene glycol (PEG-400) as a soft template and presented excellent electrochemical behavior.[203]

An advanced strategy to restrict the volume variation is to combine the core–shell Fe_3O_4@C with the mesoporous structure for its excellently large surface area and voids. Yuan *et al.* successfully produced mesoporous Fe_3O_4@C nanocapsules (Fig. 11c) by replacing the aforementioned hematite nanospindles with FeOOH nanorods.[204] Interestingly, when sintering at 500 °C a mesoporous structure was obtained, while the carbonaceous sheath was transformed to carbon shells. The mesopores in Fe_3O_4 nanorods played an important role in relieving the impact of volume change of active materials by providing more space for the volume expansion and contraction, and releasing the stress on the carbon shells. Without the buffering effects of mesopores, the carbon shells would suffer severe volumetric changes and might be destroyed during long-time and high-rate charge/discharge cycles.

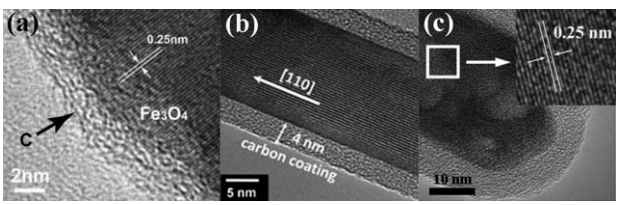

Fig. 11 TEM images of Fe_3O_4@C nanospindles (a) (Taken from ref. 202. Reproduced by permission of John Wiley and Sons), nanowires (b) (Taken from ref. 203. Reproduced by permission of the Royal Society of Chemistry), and mesoporous nanorods (c) (Taken from ref. 204(a). Reproduced by permission of the American Chemical Society).

The results presented here give clear evidence of the ability of carbon coatings to improve the electrochemical performance of nanostructured MOs as anode materials for LIBs. However, Fe_3O_4 has a relatively high electronic conductivity of 10^2 S cm^{-1}, which is very close to that of amorphous carbon. The carbon shell always occupies over 20 wt% of the obtained composites. Thus, it may be substituted with other materials to offer more active materials, higher tap densities, better initial coulombic efficiencies, *etc.*

5.2 SnO_2 with carbon shells

Owing to its high theoretical specific capacity (~780 mAh g^{-1}), SnO_2 is also regarded as one of the most promising MO anode materials to meet the requirements of next generation LIBs. The mechanism of Li storage in SnO_2 is different from Fe_3O_4 and can be expressed in eqns (8) and (9). The irreversible reaction in eqn (8) and the formation of SEI films cause a large initial irreversible capacity. Another critical problem is the serious capacity fading due to the huge volumetric variation during charge/discharge cycles, which hinders its practical application. Core–shell structures are widely used to alter this situation.

$$SnO_2 + 4Li^+ + 4e^- \rightarrow Sn + 2Li_2O \quad (8)$$

$$Sn + xLi^+ + xe^- \leftrightarrow Li_xSn\ (0 \le x \le 4.4) \quad (9)$$

In recent years, several core–shell SnO_2@C nanoparticles have been successfully fabricated through various methods and showed better electrochemical performances.[85,205–207] For a typical example, Zhang *et al.* produced 3D superstructures composed of SnO_2@C core–shell nanochains through a hydrothermal procedure.[85] The nanochain is made of perfect core–shell nanostructures with a homogenous carbon thickness of ~10 nm (see Fig. 12), in which the SnO_2 nanocores were fully coated and linearly joined one by one. The unique 3D network architecture based on core–shell nanochains presented a considerable capacity of over 600 mAh g^{-1} at a high current density of 1104 mA g^{-1}.

Core–shell SnO_2@C hollow spheres were also studied by many researchers given that the hollow structure can create a rapid lithium transportation path, accommodate the volume expansion, and hence facilitate the high-rate capability, while the carbon shell offers better electronic conductivity.[208–210] Lou *et al.* prepared coaxial SnO_2@C nanospheres with a SiO_2 template under hydrothermal conditions, and the template was removed in an alkaline solution.[209] Furthermore, Lin *et al.* synthesized

hollow SnO_2@C nanospheres *via* two steps of hydrothermal treatments.[210] The carbon–coated SnO_2 hollow nanospheres with ultrathin SnO_2 inner shell demonstrated an outstanding cycling performance at high rates.

Besides, the core–shell structure can incorporate with 1D nanomaterials to obtain SnO_2@C nanofibers,[211] CNT@SnO_2@C nanocables,[212] and SnO_2@V_2O_5 nanowires[213] with high-rate capabilities. All of the results prove that the carbon shell plays a positive role in improving the electrochemical performance of SnO_2 anode materials, especially when combining with hollow, 1D, or mesoporous structures.

5.3 TiO_2 with carbon shells

Different from the general conversion mechanism of MO anodes, TiO_2 is a typical Li^+ intercalation compound. The reaction can be expressed as: $TiO_2 + xLi^+ + xe^- \leftrightarrow Li_xTiO_2$ ($0 \le x \le 1$), which causes a small volume variation (<4%), and this is critical for the high-rate capability and long-life cycling. Furthermore, TiO_2 can offer a lower voltage (1.5 V *vs.* Li^+/Li) than that of $Li_4Ti_5O_{12}$ (~1.9 V *vs.* Li^+/Li). However, the intrinsically low electronic conductivity of TiO_2 as an n-type semiconductor hinders its performance to a great extent. Mixing as-prepared TiO_2 with highly conductive materials such as C,[214] Sn,[60] and PANI[215] can effectively solve this problem, especially incorporating with core–shell structures. For instance, TiO_2@Sn core–shell nanotubes were prepared by Kim *et al.* through thermal decomposition of $SnCl_4$ on TiO_2 nanotubes at 300 °C.[60] The obtained core–shell materials demonstrated a superior Li storage capability of 176 mAh g^{-1} even at high current rate of 4000 mA g^{-1}.

5.4 Other oxides with carbon shells

Besides the aforementioned Fe_3O_4, SnO_2, and TiO_2, a variety of MOs have been investigated in depth as anode materials in LIBs.[216–222] However, only a few can be assembled with carbon materials, because the high-valence metal can be reduced under the H_2 or CO atmosphere released during the traditional carbonization of polysaccharides at high temperatures (generally >400 °C).[72] For example, Fe_2O_3, Co_3O_4, MnO_2, MoO_3, CuO, and NiO can be gradually reduced into Fe_3O_4, CoO, MnO, MoO_2, Cu_2O and Ni metal, respectively. Higher temperatures can also lead to the formation of counterpart metals. Following this line, some MO@C composites such as Fe_3O_4@C,[202] and MnO@C,[220] can be obtained from high-valence transition metal oxides coated with carbon precursors. Surely, decreasing the annealing temperatures can achieve both the MO core with high valence and carbon shell simultaneously. For example, MoO_3@C nanobelts were produced through a hydrothermal technique followed by a heat treatment at 265 °C for 3 h in air.[216] The final product presented a significantly enhanced cyclic stability and specific capacity of 1064 mAh g^{-1} at the 50th cycle. The excellent performance may arise from the carbon coating on the nanobelts.

It is exciting that, more recently, SnO_2@C nanochains have been realized at a relatively high temperature (700 °C) through a low argon flow rate, during which trace oxygen was controllably released to maintain a chemical equilibrium for the following possible reaction process: $SnO_2 \leftrightarrow SnO \leftrightarrow Sn$.[223] This low-flow-rate protecting concept enlightens us on preparing high-valance MOs@C composites.

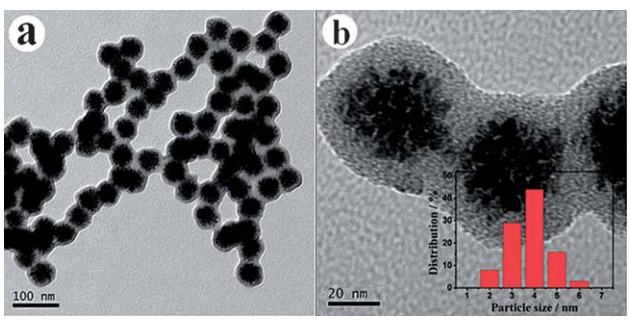

Fig. 12 Typical TEM images of SnO_2@C nanochain-built superstructures. (Taken from ref. 85. Reproduced by permission of the Royal Society of Chemistry).

6. Graphene as shell

Graphene, a one-atom-thick monolayer consisting of carbon atoms tightly packed into a two dimensional (2D) honeycomb sp^2 carbon lattice, exhibits excellent electronic transport properties. It behaves like a metal with an almost high constant mobility over a large range of temperatures and charge densities. In addition, GNSs possess an open porous system which makes the material flexible due to the lack of rigid connections between adjacent nanosheets. This flexible porous system could be used as a confining structure with substantial buffering capability to reduce electrode pulverization. Furthermore, GNSs also have a maximal surface area of ~2600 m^2 g^{-1}, and good thermal and mechanical stability.[30,75,224,225] In comparison with amorphous carbon, graphite, MCMB, and CNTs, graphene-based materials show better electronic capability and cyclic stability because of the above mentioned advantages, and hence become hot topics in the field of LIBs. Almost all the promising anode materials, including Si,[53,226] Sn,[227] Fe_3O_4,[228–231] SnO_2,[225,232–234] TiO_2,[235] and MoS_2,[236] have been introduced into graphene-based systems. Another great advantage in graphene-based materials is that the preparation routes successfully avoid heat treatments under high temperatures in comparison with traditional carbon coating from polysaccharide pyrolysis, which can reduce some MOs (such as Co_3O_4,[237,238] CuO,[239] Fe_2O_3,[240,241] Mn_3O_4[242]) into low-valence oxides and even metals. However, active particles between GNSs tend to aggregate into larger particles during cycling processes and hence cause obvious electrochemical degradation. To encapsulate active materials with GNSs instead of simple mixing can effectively solve this problem, whereas the achievement of both electronic conductivity and an ultra thin layer is still a large challenge.

Recently, Yang and coworkers introduced a novel strategy to prepare graphene-encapsulated metal oxides through the coassembly of negatively charged graphene oxides and positively charged oxide nanoparticles.[243] The process is driven by the mutual electrostatic interactions of the two species, followed by chemical reduction. The overall synthetic procedure involves three steps (Fig. 13a). Oxide nanoparticles were first decorated by surface grafting of aminopropyltrimethoxysilane (APS) to render the oxide surface positively charged. The modified oxide

nanoparticles were then assembled with negatively charged graphene oxide by electrostatic interaction. Under optimal conditions, almost all the graphene oxides and modified oxide nanoparticles coassembled to leave a transparent aqueous solution. Finally, the resulting aggregates were chemically reduced with hydrazine to result in graphene-encapsulated oxide nanoparticles (Fig. 13b). The resulting graphene-encapsulated metal oxides possessed flexible and ultrathin graphene shells that effectively enwrapped the oxide nanoparticles. This unique hybrid architecture can suppress the aggregation of oxide nanoparticles, accommodate the volume change during the cycle processes, give rise to high oxide contents in the composite of up to 91.5 wt%, and maintain the high electrical conductivity of the overall electrode. As a typical example, the as-prepared graphene-encapsulated Co_3O_4 composites presented very high reversible capacities of about 1100 mAh g^{-1} in the initial 10 cycles and 1000 mAh g^{-1} after 130 cycles at 74 mA g^{-1}, which were much higher than those of all Co_3O_4 electrodes reported to date (600–850 mAh g^{-1}). Similarly, graphene-encapsulated Co_3O_4 composites were fabricated through the chemical decomposition method[237] and microwave-assisted synthesis.[238]

It is reasonable to speculate that the GNS shell is not a completely coating layer, but a percolated film instead. Otherwise, Li^+ ions can not percolate into the active core. This hypothesis can be proved by Wang's work to some extent. Wang *et al.* fabricated carbon nanocages with nanographene shells by a catalytic decomposition of *p*-xylene over a Co/Mo catalyst in supercritical carbon dioxide and discovered high reversible capacities, superior rate performances, and good cyclic stability.[244] N_2 adsorption/desorption analyses of these carbon nanocages revealed the presence of fine pores, with a mean diameter of about 2.3 nm, and large mesopores. The large intercage mesopores, together with the fine pores in the cage shell, form a network, facilitating the diffusion of electrolyte into the cages, and thus the fast transportation of ions, which can be illustrated in Fig. 14. Another powerful evidence is the interleaved graphene-encapsulated Fe_3O_4 composite prepared by Zhou and coworkers.[231] In this system, Fe_3O_4 particles were wrapped with a well-proportioned and ultrathin GNS layer and presented a reversible specific capacity approaching 1026 mAh g^{-1} after 30 cycles at 35 mA g^{-1} and 580 mAh g^{-1} after 100 cycles at 700 mA g^{-1}. The excellent performance can be ascribed to the flexible interleaved structure for tolerating the volume change and preventing the detachment and agglomeration of pulverized Fe_3O_4 particles during cycling. The GNS shell also acts as an electron transport highway for improving the electrical

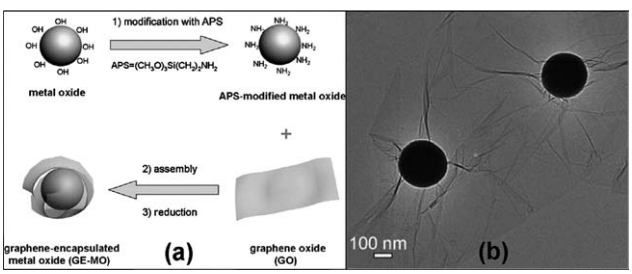

Fig. 13 A schematic illustration (a) and TEM image (b) of graphene-encapsulated Co_3O_4. (Taken from ref. 243. Reproduced by permission of John Wiley and Sons).

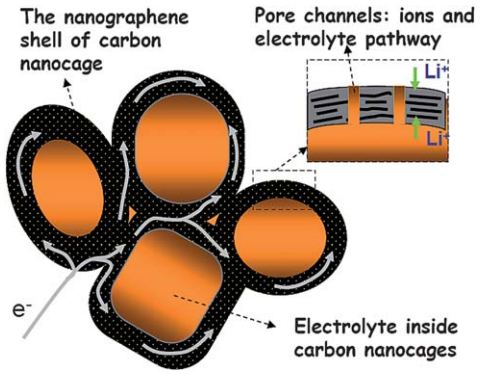

Fig. 14 Schematic representations of electron transportation and Li ion diffusion in the carbon shell, and electrolyte penetration within the porous network of the carbon nanocages. (Taken from ref. 244. Reproduced by permission of the Royal Society of Chemistry).

conductivity, whereas the Fe_3O_4 particles inhibit the restacking of GNSs. More importantly, the flexible interleaved structure contains some large-size porosity that can also facilitate fast ion transport.

Additionally, this strategy has been successfully applied in cathode materials very recently.[245–247] Zhou *et al.* produced graphene-modified $LiFePO_4$ cathode materials with excellent high-rate capabilities and cycling stability by using a spray-drying technique.[245] The outer GNSs were loosely wrapped on $LiFePO_4$ nanoparticles, while GNSs inside the microspheres were integrated into a continuous 3D conductive network. In this system, electrons can be easily transferred between the surface of $LFePO_4$ nanocrystals and GNSs, and move rapidly over the nanoparticles to attain a high rate capability.

Note that the practical GNS is usually not a perfectly infinite 2D monolayer and possesses great distorted sp^2 nanodomains, edges or other defects, which can also store Li^+ and present a considerable capacity. Pan *et al.* succeeded in preparing GNSs with controllable structure parameters by hydrazine reduction, low temperature pyrolysis and electron beam irradiation, and systematically investigated their Li storage properties.[248] They discovered that highly disordered GNSs showed a high electrochemical capacity of ~800 mAh g^{-1} after 15 cycles and good cycling stability. The enhanced capacity in disordered GNSs was mainly ascribed to additional reversible storage sites such as edges and other defects. However, the defects can also bring poor electronic conductivity, and the larger specific surface area may lead to a higher irreversible capacity. Therefore, it is necessary to balance the Li storage capacity and electronic conductivity.

Over all, graphene-encapsulated active materials have been developed into a feasible and promising strategy to improve the electrochemical behavior, especially the high-rate performance for future LIBs. Continued efforts are now ongoing to push the GNS additives for practical applications in LIBs, especially in the high-power cases where a more effective conducting network with much less additive is expected.

7. Conclusion and prospective

Since their successful commercialization in 1990s, LIBs have been greatly developed in both electrochemical capability and

industrial technique. Great efforts have been made in exploring advanced active materials with improved performance in terms of high energy/power density, good mechanical/thermal stability, environmental friendliness, and low cost for practical applications. To accomplish these goals, researchers have been developing various feasible strategies, including optimizing the crystalline lattice of active materials by doping cations or anions, reducing particles to a suitable scale to offer enhanced electron/Li^+ ion conductivity and reactivity, combining active materials and other active/inactive materials together for complementary strengthening, especially when assembled into core–shell structures.

In core–shell systems, the shell layer always plays an important role in improving the electrochemical performance of active materials in many terms. Firstly, the shell enhances the electronic conductivity not only over the surface of active cores but also between the current collector and active materials as well as the interconnection among active particles. Secondly, the shell offers an elastic buffering space for the huge expansion/contraction, especially for anode materials. Thirdly, the shell prevents the sensitively active cores from directly contacting the outside environment (air or electrolytes) and then avoiding or restricting the co-insertion of solvent molecules and loss of active compositions. Finally, the shell also works as a HF scavenger to react with HF released from electrolytes prior to active cores, and hence maintains a high and stable performance. For one of the above functions, many materials beyond carbon can be selected as shell materials. To enhance electronic conductivity, highly-conductive materials are suitable, such as carbon materials, electrically conductive polymers, metals, and metal oxides (RuO_2 and CeO_2). To accommodate the volume variation, amorphous carbon, polymers, GNSs, and other flexible materials are good, and are better when they are filled with pores. To act as a physical protection layer, stable and dense inactive materials (such as oxides and fluorides) can be chosen; meanwhile Li^+ ion can percolate across these materials. To work as HF scavengers, ideal candidates (Al_2O_3, ZrO_2, *etc.*) should react with Li^+ more easily and simultaneously form a stable and thin layer to prevent further erosion. Additionally, a well-proportioned coating shell with different materials calls for various preparation techniques.

Although core–shell structures have been extensively and intensively investigated in LIBs, there are still some obstacles. For layered $LiMO_2$, spinel-type $LiMn_2O_4$, and HTMOs, they are easily reduced when encapsulated with pyrolyzed carbon materials at high temperatures. Oxides, fluorides, and phosphates can substitute for carbon materials to decorate the active material surface and show enhanced electrochemical performance. However, the inherently poor electronic conductivity hampers their practical utilization. To restrict the huge volume variation of anodes, the coating layers usually occupy a weight of 20% in the composites. More inactive materials or an active material with lower Li storage will lead to a lower specific capacity. Though smaller active material particles are beneficial for the coating treatment and subsequently better electrochemical performances, nanomaterials can bring low tap densities and high cost. Correspondingly, there are some promising prospects enlightened by all the previous reports, which can guide the direction for future efforts. Novel techniques should be developed to control the reaction time and atmosphere so as to avoid reduction of high-valence metals. Ultra thin oxide coating techniques including ALD may be further explored in depth considering their excellent capability. DCC techniques can be adopted in more nanomaterials to obtain both high reversible capacities and high tap densities. Graphene-encapsulated active materials are more attractive, due to the maximal surface area, high electronic conductivity, flexibility, low content in composites. More studies should focus on exploring advanced core–shell structures and revealing the modification mechanism. Finally, the practical utilization of nanomaterials needs more efforts on large-scale production and new industrial techniques in the future.

Acknowledgements

This work was supported by the 973 Program (2009CB220100) and MOE NCET (08–0293) as well as Innovation Research Team (IRT0927) in China.

Notes and references

1 C. Liu, F. Li, L. P. Ma and H. M. Cheng, *Adv. Energy Mater.*, 2010, **22**, E28–E62.
2 Z. Yang, J. Zhang, M. C. W. Kintner-Meyer, X. Lu, D. Choi, J. P. Lemmon and J. Liu, *Chem. Rev.*, 2011, **111**, 3577–3613.
3 H.-K. Song, K. T. Lee, M. G. Kim, L. F. Nazar and J. Cho, *Adv. Funct. Mater.*, 2010, **20**, 3818–3834.
4 J. B. Goodenough and Y. Kim, *Chem. Mater.*, 2010, **22**, 587–603.
5 H. Li, Z. Wang, L. Chen and X. Huang, *Adv. Mater.*, 2009, **21**, 4593–4607; D. H. Wu and Z. Zhou, *Frontiers of Physics*, 2011, **6**, 197–203.
6 P. G. Bruce, B. Scrosati and J.-M. Tarascon, *Angew. Chem., Int. Ed.*, 2008, **47**, 2930–2946.
7 A. S. Aricò, P. Bruce, B. Scrosati, J.-M. Tarascon and W. V. Schalkwijk, *Nat. Mater.*, 2005, **4**, 366–377.
8 P. Reiss, M. Protière and L. Li, *Small*, 2009, **5**, 154–168.
9 H. Zeng, J. Li, Z. L. Wang, J. P. Liu and S. H. Sun, *Nano Lett.*, 2004, **4**, 187–190.
10 F. Caruso, *Adv. Mater.*, 2001, **13**, 11–22.
11 Y. Wang, A. S. Angelatos and F. Caruso, *Chem. Mater.*, 2008, **20**, 848–858.
12 J. Luo, L. Wang, D. Mott, P. N. Njoki, Y. Lin, T. He, Z. Xu, B. N. Wanjana, I. I. S. Lim and C.-J. Zhong, *Adv. Mater.*, 2008, **20**, 4342–4347.
13 X. C. Xiao, L.-Y. Chu, W. M. Chen, S. Wang and Y. Li, *Adv. Funct. Mater.*, 2003, **13**, 847–852.
14 Y. Zhu, J. Shi, W. Shen, X. Dong, J. Feng, M. Ruan and Y. Li, *Angew. Chem., Int. Ed.*, 2005, **44**, 5083–5087.
15 G.-R. Li, Z.-L. Wang, F.-L. Zheng, Y.-N. Ou and Y.-X. Tong, *J. Mater. Chem.*, 2011, **21**, 4217–4221.
16 J.-H. Kim, S. H. Kang, K. Zhu, J. Y. Kim, N. R. Neale and A. J. Frank, *Chem. Commun.*, 2011, **47**, 5214–5216.
17 M. M. Ren, Z. Zhou, X. P. Gao and J. Yan, *Prog. Chem.*, 2008, **20**, 771–777.
18 L. M. Liz-Marzán, M. Giersig and P. Mulvaney, *Langmuir*, 1996, **12**, 4329–4335.
19 S. Liu and M.-Y. Han, *Chem. Asian J.*, 2010, **5**, 36–45.
20 S.-H. Hu and X. Gao, *Adv. Funct. Mater.*, 2010, **20**, 3721–3726.
21 X. W. Lou, C. L. Yuan, E. Rhoades, Q. Zhang and L. A. Archer, *Adv. Funct. Mater.*, 2006, **16**, 1679–1684.
22 F. Zhang, G. B. Braun, Y. F. Shi, Y. C. Zhang, X. H. Sun, N. O. Reich, D. Y. Zhao and G. Stucky, *J. Am. Chem. Soc.*, 2010, **132**, 2850–2851.
23 S. H. Joo, J. Y. Park, C. K. Tsung, Y. Yamada, P. D. Yang and G. A. Somorjai, *Nat. Mater.*, 2009, **8**, 126–131.
24 Q. Cao, H. Zhang, G. Wang, Q. Xia, Y. Wu and H. Wu, *Electrochem. Commun.*, 2007, **9**, 1228–1232.
25 J. Xie, N. Imanishi, T. Matsumura, A. Hirano, Y. Takeda and O. Yamamoto, *Solid State Ionics*, 2008, **179**, 362–370.
26 Y. Koyama, T. E. Chin, U. Rhyner, R. K. Holman, S. R. Hall and Y. M. Chiang, *Adv. Funct. Mater.*, 2006, **16**, 492–498.

27 Y. M. Chiang, H. Wang and Y. Jang, *Chem. Mater.*, 2001, **13**, 53–56.
28 T. I. F. Munakata, Y. Ohsawa and M. Kawai, *J. Mater. Sci. Lett.*, 2002, **21**, 117–119.
29 A. R. Armstrong and P. G. Bruce, *Nature*, 1996, **381**, 499–500.
30 D. Chen, L. Tang and J. Li, *Chem. Soc. Rev.*, 2010, **39**, 3157–3180.
31 J. Molenda, M. Ziemnicki, J. Marzec, W. Zajac, M. Molenda and M. Bucko, *J. Power Sources*, 2007, **173**, 707–711.
32 K. S. J. Molenda, W. Kucza, J. Marzec and A. Stoklosa, *Solid State Ionics*, 1999, **123**, 155–163.
33 M. S. K. Zaghib, M. Armand and M. Gauthier, *J. Power Sources*, 1999, **81–82**, 300–305.
34 C. H. Chen, J. T. Vaughey, A. N. Jansen, D. W. Dees, A. J. Kahaian, T. Goacher and M. M. Thackeray, *J. Electrochem. Soc.*, 2001, **148**, A102–A104.
35 Z. Yang, D. Choi, S. Kerisit, K. M. Rosso, D. Wang, J. Zhang, G. Graff and J. Liu, *J. Power Sources*, 2009, **192**, 588–598.
36 S.-Y. Chung, J. T. Bloking and Y.-M. Chiang, *Nat. Mater.*, 2002, **1**, 123–128.
37 H. Liu, C. Li, H. Zhang, L. Fu, Y. Wu and H. Wu, *J. Power Sources*, 2006, **159**, 717–720.
38 K. S. N. A. K. Padhi and J. B. Goodenough, *J. Electrochem. Soc.*, 1997, **144**, 1188–1194.
39 M. L. Marcinek, J. W. Wilcox, M. M. Doeff and R. M. Kostecki, *J. Electrochem. Soc.*, 2009, **156**, A48–A51.
40 D. Wang, X. Wu, Z. Wang and L. Chen, *J. Power Sources*, 2005, **140**, 125–128.
41 C. Delacourt, L. Laffont, R. Bouchet, C. Wurm, J. B. Leriche, M. Morcrette, J. M. Tarascon and C. Masquelier, *J. Electrochem. Soc.*, 2005, **152**, A913–A921.
42 D. Morgan, A. van der Ven and G. Ceder, *Electrochem. Solid-State Lett.*, 2004, **7**, A30–A32.
43 A. Yamada, *J. Power Sources*, 2003, **119–121**, 232–238.
44 M. Yonemura, A. Yamada, Y. Takei, N. Sonoyama and R. Kanno, *J. Electrochem. Soc.*, 2004, **151**, A1352–A1356.
45 P. Deniard, A. M. Dulac, X. Rocquefelte, V. Grigorova, O. Lebacq, A. Pasturel and S. Jobic, *J. Phys. Chem. Solids*, 2004, **65**, 229–233.
46 K. N. Natalia, N. Bramnik, C. Baehtz, K. G. Bramnik and H. Ehrenberg, *Chem. Mater.*, 2007, **19**, 908–915.
47 J. Wolfenstine, *J. Power Sources*, 2006, **158**, 1431–1435.
48 N. Bramnik, K. Bramnik, C. Baehtz and H. Ehrenberg, *J. Power Sources*, 2005, **145**, 74–81.
49 S.-C. Yin, P. S. Strobel, H. Grondey and L. F. Nazar, *Chem. Mater.*, 2004, **16**, 1456–1465.
50 H. O. M. Sato, K. Yoshida, M. Saito, K. Uematsu and K. Toda, *Solid State Ionics*, 2000, **135**, 137–142.
51 S. Patoux, C. Wurm, M. Morcrette, G. Rousse and C. Masquelier, *J. Power Sources*, 2003, **119–121**, 278–284.
52 T. Zhang, L. Fu, J. Gao, L. Yang, Y. Wu and H. Wu, *Pure Appl. Chem.*, 2006, **78**, 1889–1896.
53 X.-L. Wang and W.-Q. Han, *ACS Appl. Mater. Interfaces*, 2010, **2**, 3709–3713.
54 K. Wang, X. He, L. Wang, J. Ren, C. Jiang and C. Wan, *Solid State Ionics*, 2007, **178**, 115–118.
55 Y. Xu, G. Yin and P. Zuo, *Electrochim. Acta*, 2008, **54**, 341–345.
56 M. Winter and J. O. Besenhard, *Electrochim. Acta*, 1999, **45**, 31–50.
57 A. E. Berkowitz, J. M. D. Coey, L. Balcells, F. F. Putris and F. T. Parker, *Appl. Phys. Lett.*, 1998, **72**, 734–736.
58 Y.-D. Ko, J.-G. Kang, K. J. Choi, J.-G. Park, J.-P. Ahn, K. Y. Chung, K.-W. Nam, W.-S. Yoon and D.-W. Kim, *J. Mater. Chem.*, 2009, **19**, 1829–1935.
59 J. H. Yu and G. M. Choi, *Sens. Actuators, B*, 2011, **75**, 56–61.
60 H. Kim, M. Kim, T. Shin, H. Shin and J. Cho, *Electrochem. Commun.*, 2008, **10**, 1669–1672.
61 S. Södergren, H. Lindström, A. Solbrand, H. Rensmo, J. Hjelm, A. Hagfeldt and S.-E. Lindquist, *J. Phys. Chem. B*, 1997, **101**, 7717–7722.
62 M. L. Sushko, K. M. Rosso and J. Liu, *J. Phys. Chem. C*, 2010, **114**, 20277–20283.
63 P. Yu, B. N. Popov, J. A. Ritter and R. E. White, *J. Electrochem. Soc.*, 1999, **146**, 8–14.
64 V. A. Sethuraman, K. Persson, L. J. Hardwick, Y. Hinuma, Y. S. Meng, A. van der Ven, V. Srinivasan, R. Kostecki and G. Ceder, *J. Phys. Chem. Lett.*, 2010, **1**, 1176–1180.
65 R. A. Serway, *Principles of Physics*, Fort Worth, Texas; London: Saunders College Publishing, 1998.
66 Y. Pauleau, P. B. Barna, *Protective coatings and thin films: synthesis, characterization, and applications*, Springer, 1997.
67 J. W. Long, K. E. Swider, C. I. Merzbacher and D. R. Rolison, *Langmuir*, 1999, **15**, 780–785.
68 H.-X. Ji, X.-L. Wu, L.-Z. Fan, C. Krien, I. Fiering, Y.-G. Guo, Y. Mei and O. G. Schmidt, *Adv. Mater.*, 2010, **22**, 4591–4595.
69 P. Balaya, H. Li, L. Kienle and J. Maier, *Adv. Funct. Mater.*, 2003, **13**, 621–625.
70 H. Schäfer, G. Schneidereit and W. Gerhardt, *Z. Anorg. Allg. Chem.*, 1963, **319**, 327–336.
71 E. Yoo, J. Kim, E. Hosono, H. S. Zhou, T. Kudo and I. Honma, *Nano Lett.*, 2008, **8**, 2277–2282.
72 Z. Chen, Y. Qin, K. Amine and Y. K. Sun, *J. Mater. Chem.*, 2010, **20**, 7606–7612.
73 J. Kim, G. Cheruvally, J. Choi, J. Ahn, G. Cho, K. Kim and H. Ahn, *J. Power Sources*, 2007, **166**, 211–218.
74 S. Shi, L. Liu, C. Ouyang, D.-S. Wang, Z. Wang, L. Chen and X. Huang, *Phys. Rev. B: Condens. Matter*, 2003, **68**, 195108.
75 Y. Q. Sun, Q. Wu and G. Shi, *Energy Environ. Sci.*, 2011, **4**, 1113–1132.
76 C. N. R. Rao, A. K. Sood, K. S. Subrahmanyam and A. Govindaraj, *Angew. Chem., Int. Ed.*, 2009, **48**, 7752–7777.
77 Y. N. Jo, Y. Kim, J. S. Kim, J. H. Song, K. J. Kim, C. Y. Kwag, D. J. Lee, C. W. Park and Y. J. Kim, *J. Power Sources*, 2010, **195**, 6031–6036.
78 Y. Wang and J. Y. Lee, *J. Power Sources*, 2005, **144**, 220–225.
79 Z. Y. Tang and Y. L. Ruan, *Acta Chim. Sin.*, 2005, **63**, 1500–1504.
80 H. Kawaoka, M. Hibino, H. Zhou and I. Honma, *Solid State Ionics*, 2005, **176**, 621–627.
81 G. X. Wang, J. Yao and H. K. Liu, *Electrochem. Solid-State Lett.*, 2004, **7**, A250–A253.
82 M. M. Ren, Z. Zhou, X. P. Gao, W. X. Peng and J. P. Wei, *J. Phys. Chem. C*, 2008, **112**, 5689–5693.
83 C. S. Sun, Z. Zhou, Z. G. Xu, D. G. Wang, J. P. Wei, X. K. Bian and J. Yan, *J. Power Sources*, 2009, **193**, 841–845; Y. Zhang, C. S. Sun and Z. Zhou, *Electrochem. Commun.*, 2009, **11**, 1183–1186.
84 L. W. Su, Z. Zhou and M. M. Ren, *Chem. Commun.*, 2010, **46**, 2590–2592.
85 B. Zhang, X. Yu, C. Ge, X. Dong, Y. Fang, Z. Li and H. Wang, *Chem. Commun.*, 2010, **46**, 9188–9190.
86 P. F. Gao, J. W. Fu, J. Yang, R. G. Lv, J. L. Wang, Y. N. Nuli and X. Z. Tang, *Phys. Chem. Chem. Phys.*, 2009, **11**, 11101–11105.
87 J. Cho, J. Lee, B. Kim, T. Kim, J. Kim and B. Park, *Electrochim. Acta*, 2005, **50**, 4182–4187.
88 G. Li, Z. X. Yang and W. S. Yang, *J. Power Sources*, 2008, **183**, 741–748.
89 Y. K. Sun, S. T. Myung, B. C. Park and K. Amine, *Chem. Mater.*, 2006, **18**, 5159–5163.
90 L. Cheng, J. Yan, G. N. Zhu, J. Y. Luo, C. X. Wang and Y. Y. Xia, *J. Mater. Chem.*, 2010, **20**, 595–602.
91 D. Deng and J. Y. Lee, *J. Mater. Chem.*, 2010, **20**, 8045–8049.
92 M. Yoshio, H. Y. Wang, K. Fukuda, T. Abe and Z. Ogumi, *Chem. Lett.*, 2003, **32**, 1130–1131.
93 H. H. Li, J. Jin, J. P. Wei, Z. Zhou and J. Yan, *Electrochem. Commun.*, 2009, **11**, 95–98.
94 I. D. Scott, Y. S. Jung, A. S. Cavanagh, Y. Yan, A. C. Dillon, S. M. George and S.-H. Lee, *Nano Lett.*, 2011, **11**, 414–418.
95 Y. S. Jung, A. S. Cavanagh, L. A. Riley, S.-H. Kang, A. C. Dillon, M. D. Groner, S. M. George and S.-H. Lee, *Adv. Mater.*, 2010, **22**, 2172–2176.
96 T. Zhang, L. J. Fu, J. Gao, L. C. Yang, Y. P. Wu and H. Q. Wu, *Pure Appl. Chem.*, 2006, **78**, 1889–1896.
97 Y. Wang, Y. Wang, E. Hosono, K. Wang and H. Zhou, *Angew. Chem., Int. Ed.*, 2008, **47**, 7461–7465.
98 S.-H. Ng, J. Wang, D. Wexler, K. Konstantinov, Z.-P. Guo and H.-K. Liu, *Angew. Chem., Int. Ed.*, 2006, **45**, 6896–6899.
99 B. L. Cushing and J. B. Goodenough, *Solid State Sci.*, 2002, **4**, 1487–1493.
100 M. M. Rahman, J.-Z. Wang, M. F. Hassan, S. Chou, Z. Chen and H. K. Liu, *Energy Environ. Sci.*, 2011, **4**, 952–957.
101 M. Jo, Y. K. Lee, K. M. Kim and J. Cho, *J. Electrochem. Soc.*, 2010, **157**, A841–A845.
102 K. S. Lee, S. T. Myung, K. Amine, H. Yashiro and Y. K. Sun, *J. Mater. Chem.*, 2009, **19**, 1995–2005.

103 Y. K. Sun, K. J. Hong, J. Prakash and K. Amine, *Electrochem. Commun.*, 2002, **4**, 344–348.
104 H. Sahan, H. Goktepe, S. Patat and A. Ulgen, *Solid State Ionics*, 2010, **181**, 1437–1444.
105 D. Arumugam and G. P. Kalaignan, *Electrochim. Acta*, 2010, **55**, 8709–8716.
106 H. B. Kang, S. T. Myung, K. Amine, S. M. Lee and Y. K. Sun, *J. Power Sources*, 2010, **195**, 2023–2028.
107 H. Sahan, H. Goktepe, S. Patat and A. Ulgen, *Solid State Ionics*, 2008, **178**, 1837–1842.
108 L. Cheng, X. L. Li, H. J. Liu, H. M. Xiong, P. W. Zhang and Y. Y. Xia, *J. Electrochem. Soc.*, 2007, **154**, A692–A697.
109 L. Cheng, H. J. Liu, J. J. Zhang, H. M. Xiong and Y. Y. Xia, *J. Electrochem. Soc.*, 2006, **153**, A1472–A1477.
110 C. Jiang, M. Ichihara, I. Honma and H. S. Zhou, *Electrochim. Acta*, 2007, **52**, 6470–6475.
111 C. H. Jiang, E. Hosono, M. Ichihara, I. Honma and H. S. Zhou, *J. Electrochem. Soc.*, 2008, **155**, A553–A556.
112 Y. Li, G. L. Pan, J. W. Liu and X. P. Gao, *J. Electrochem. Soc.*, 2009, **156**, A495–A499.
113 H. Zhang, L. Qi, X. P. Gao, K. Yang and D. Zhang, *Chin. J. Inorg. Chem.*, 2010, **26**, 1539–1543.
114 Y. G. Wang, H. M. Liu, K. X. Wang, H. Eiji, Y. R. Wang and H. S. Zhou, *J. Mater. Chem.*, 2009, **19**, 6789–6795.
115 J. Gao, C. Y. Jiang and C. R. Wan, *J. Electrochem. Soc.*, 2010, **157**, K39–K42.
116 R. Cai, X. Yu, X. Liu and Z. Shao, *J. Power Sources*, 2010, **195**, 8244–8250.
117 N. Zhu, W. Liu, M. Q. Xue, Z. A. Xie, D. Zhao, M. N. Zhang, J. T. Chen and T. B. Cao, *Electrochim. Acta*, 2010, **55**, 5813–5818.
118 S.-T. Myung, K. Izumi, S. Komaba, Y.-K. Sun, H. Yashiro and N. Kumagai, *Chem. Mater.*, 2005, **17**, 3695–3704.
119 D. Aurbach, E. Zinigrad, Y. Cohen and H. Teller, *Solid State Ionics*, 2002, **148**, 405–416.
120 K. Xu, S. S. Zhang, T. R. Jow and T. B. Curtis, *J. Phys. Chem. C*, 2007, **111**, 7411–7421.
121 D. Lu, W. Li, X. Zuo, Z. Yuan and Q. Huang, *J. Phys. Chem. C*, 2007, **111**, 12067–12074.
122 M. Q. Xu, L. D. Xing and W. S. Li, *Prog. Chem.*, 2009, **21**, 2017–2027.
123 J. Cho, C.-S. Kim and S.-I. Yoo, *Electrochem. Solid-State Lett.*, 2000, **3**, 362–365.
124 J. Cho, Y. J. Kim and B. Park, *Chem. Mater.*, 2000, **12**, 3788–3791.
125 J. Cho, Y. J. Kim, T.-J. Kim and B. Park, *Angew. Chem., Int. Ed.*, 2001, **40**, 3367–3369.
126 J. Cho, Y. J. Kim and B. Park, *J. Electrochem. Soc.*, 2001, **148**, A1110–A1115.
127 Z. Chen and J. R. Dahn, *Electrochem. Solid-State Lett.*, 2002, **5**, A213–A216.
128 L. J. Liu, L. Q. Chen, X. J. Huang, X. Q. Yang, W. S. Yoon, H. S. Lee and J. McBreen, *J. Electrochem. Soc.*, 2004, **151**, A1344–A1351.
129 Z. Chen and J. R. Dahn, *Electrochem. Solid-State Lett.*, 2003, **6**, A221–A224.
130 A. M. Kannan, L. Rabenberg and A. Manthiram, *Electrochem. Solid-State Lett.*, 2003, **6**, A16–A18.
131 S. K. Hu, G. H. Cheng, M. Y. Cheng, B. J. Hwang and R. Santhanam, *J. Power Sources*, 2009, **188**, 564–569.
132 B. J. Hwang, C. Y. Chen, M. Y. Cheng, R. Santhanam and K. Ragavendran, *J. Power Sources*, 2010, **195**, 4255–4265.
133 D. Q. Liu, X. Q. Liu and Z. Z. He, *J. Alloys Compd.*, 2007, **436**, 387–391.
134 R. Singhal, M. S. Tomar, J. G. Burgos and R. S. Katiyar, *J. Power Sources*, 2008, **183**, 334–338.
135 A. Basch and J. H. Albering, *J. Power Sources*, 2011, **196**, 3290–3295.
136 F. Wu, M. Wang, Y. F. Su, L. Y. Bao and S. Chen, *Electrochim. Acta*, 2009, **54**, 6803–6807.
137 S. T. Myung, K. S. Lee, C. S. Yoon, Y. K. Sun, K. Amine and H. Yashiro, *J. Phys. Chem. C*, 2010, **114**, 4710–4718.
138 Y. K. Sun, J. M. Han, S. T. Myung, S. W. Lee and K. Amine, *Electrochem. Commun.*, 2006, **8**, 821–826.
139 Y. K. Sun, S. W. Cho, S. T. Myung, K. Amine and J. Prakash, *Electrochim. Acta*, 2007, **53**, 1013–1019.
140 S. U. Woo, C. S. Yoon, K. Amine, I. Belharouak and Y. K. Sun, *J. Electrochem. Soc.*, 2007, **154**, A1005–A1009.
141 H. B. Kim, B. C. Park, S. T. Myung, K. Amine, J. Prakash and Y. K. Sun, *J. Power Sources*, 2008, **179**, 347–350.
142 B. C. Park, H. B. Kim, S. T. Myung, K. Amine, I. Belharouak, S. M. Lee and Y. K. Sun, *J. Power Sources*, 2008, **178**, 826–831.
143 Y. K. Sun, C. S. Yoon, S. T. Myung, I. Belharouak and K. Amine, *J. Electrochem. Soc.*, 2009, **156**, A1005–A1010.
144 J. G. Li, L. Wang, Q. Zhang and X. M. He, *J. Power Sources*, 2009, **190**, 149–153.
145 S. H. Yun, K. S. Park and Y. J. Park, *J. Power Sources*, 2010, **195**, 6108–6115.
146 Y. C. Lu, A. N. Mansour, N. Yabuuchi and Y. Shao-Horn, *Chem. Mater.*, 2009, **21**, 4408–4424.
147 S. M. Lee, S. H. Oh, J. P. Ahn, W. I. Cho and H. Jang, *J. Power Sources*, 2006, **159**, 1334–1339.
148 B. Kim, C. Kim, D. Ahn, T. Moon, J. Ahn, Y. Park and B. Park, *Electrochem. Solid-State Lett.*, 2007, **10**, A32–A35.
149 Y. H. Chen, Z. Y. Tang, G. Q. Zhang, X. M. Zhang, R. Z. Chen, Y. G. Liu and Q. Liu, *J. Wuhan Univ. Technol., Mater. Sci. Ed.*, 2009, **24**, 347–353.
150 G. R. Hu, X. R. Deng, Z. D. Peng and K. Du, *Electrochim. Acta*, 2008, **53**, 2567–2573.
151 Y. Kim and J. Cho, *J. Electrochem. Soc.*, 2007, **154**, A495–A499.
152 H. Lee, M. Kim and J. Cho, *Electrochem. Commun.*, 2007, **9**, 149–154.
153 H. Wang, W. Zhang, L. Zhu and M. Chen, *Solid State Ionics*, 2007, **178**, 131–136.
154 S. B. Kim, K. J. Lee, W. J. Choi, W. S. Kim, I. C. Jang, H. H. Lim and Y. S. Lee, *J. Solid State Electrochem.*, 2010, **14**, 919–922.
155 W. S. Kim, S. B. Kim, I. C. Jang, H. H. Lim and Y. S. Lee, *J. Alloys Compd.*, 2010, **492**, L87–L90.
156 Y.-K. Sun, S.-T. Myung, B.-C. Park, J. Prakash, I. Belharouak and K. Amine, *Nat. Mater.*, 2009, **8**, 320–324.
157 Y. K. Sun, S. T. Myung, M. H. Kim, J. Prakash and K. Amine, *J. Am. Chem. Soc.*, 2005, **127**, 13411–13418.
158 Y. Koyama, *J. Power Sources*, 2003, **119–121**, 644–648.
159 S.-T. Myung, S. Komada, K. Kurihara, K. Hosoya, Y.-K. Sun, N. Kumaga, I. Nakai, M. Yonemura and T. Kamiyama, *Chem. Mater.*, 2006, **18**, 1658–1666.
160 Y. S. Jung, A. S. Cavanagh, A. C. Dillon, M. D. Groner, S. M. George and S.-H. Lee, *J. Electrochem. Soc.*, 2010, **157**, A75–A81.
161 B. Ellis, P. Subramanya Herle, Y. H. Rho, L. F. Nazar, R. Dunlap, L. K. Perry and D. H. Ryan, *Faraday Discuss.*, 2007, **134**, 119–141.
162 S. Ferrari, R. L. Lavall, D. Capsoni, E. Quartarone, A. Magistris, P. Mustarelli and P. Canton, *J. Phys. Chem. C*, 2010, **114**, 12598–12603.
163 Z. R. Chang, H. J. Lv, H. W. Tang, H. J. Li, X. Z. Yuan and H. J. Wang, *Electrochim. Acta*, 2009, **54**, 4595–4599.
164 S. W. Oh, S.-T. Myung, S.-M. Oh, K. H. Oh, K. Amine, B. Scrosati and Y.-K. Sun, *Adv. Mater.*, 2010, **22**, 4842–4845.
165 C. S. Sun, Y. Zhang, X. J. Zhang and Z. Zhou, *J. Power Sources*, 2010, **195**, 3680–3683.
166 X. J. Zhang, Y. Zhang, Z. Zhou, J. P. Wei, R. Essehli and B. Elbali, *Electrochim. Acta*, 2011, **56**, 2290–2294.
167 K. Zaghib, K. Striebel, A. Guerfi, J. Shim, M. Armand and M. Gauthier, *Electrochim. Acta*, 2004, **50**, 263–270.
168 Y. L. Cao, L. H. Yu, T. Li, X. P. Ai and H. X. Yang, *J. Power Sources*, 2007, **172**, 913–918.
169 Y. H. Huang, K. S. Park and J. B. Goodenough, *J. Electrochem. Soc.*, 2006, **153**, A2282–A2286.
170 S. W. Oh, S.-T. Myung, H. J. Bang, C. S. Yoon, K. Amine and Y.-K. Sun, *Electrochem. Solid-State Lett.*, 2009, **12**, A181–A185.
171 A. V. Murugan, T. Muraliganth and A. Manthiram, *J. Electrochem. Soc.*, 2009, **156**, A79–A83.
172 T. N. L. Doan, Z. Bakenov and I. Taniguchi, *Adv. Powder Technol.*, 2010, **21**, 187–196.
173 S. M. Oh, S. W. Oh, C. S. Yoon, B. Scrosati, K. Amine and Y. K. Sun, *Adv. Funct. Mater.*, 2010, **20**, 3260–3265.
174 Y. Wang, Y. Yang, Y. Yang and H. Shao, *Solid State Commun.*, 2010, **150**, 81–85.
175 T. N. L. Doan and I. Taniguchi, *J. Power Sources*, 2011, **196**, 1399–1408.
176 J. Yang and J. J. Xu, *J. Electrochem. Soc.*, 2006, **153**, A716–A523.

177 H. Huang, S. C. Yin, T. Kerr, N. Taylor and L. F. Nazar, *Adv. Mater.*, 2002, **14**, 1525–1528.
178 M. M. Ren, Z. Zhou, Y. Z. Li, X. P. Gao and J. Yan, *J. Power Sources*, 2006, **162**, 1357–1362.
179 T. Jiang, W. C. Pan, J. Wang, X. F. Bie, F. Du, Y. J. Wei, C. Z. Wang and G. Chen, *Electrochim. Acta*, 2010, **55**, 3864–3869.
180 Y. Z. Li, Z. Zhou, M. M. Ren, X. P. Gao and J. Yan, *Electrochim. Acta*, 2006, **51**, 6498–6502.
181 J. S. Huang, L. Yang, K. Y. Liu and Y. F. Tang, *J. Power Sources*, 2010, **195**, 5013–5018.
182 R. Teki, M. K. Datta, R. Krishnan, T. C. Parker, T.-M. Lu, P. N. Kumta and N. Koratkar, *Small*, 2009, **5**, 2236–2242.
183 J. R. Szczech and S. Jin, *Energy Environ. Sci.*, 2011, **4**, 56–72.
184 P. Zuo, G. Yin and Y. Ma, *Electrochim. Acta*, 2007, **52**, 4878–4883.
185 U. Kasavajjula, C. Wang and A. Appleby, *J. Power Sources*, 2007, **163**, 1003–1039.
186 Y. Kang, M. Park, J. Lee and H. Liu, *Carbon*, 2007, **45**, 1928–1933.
187 S. H. Ng, J. Wang, D. Wexler, S. Y. Chew and H. K. Liu, *J. Phys. Chem. C*, 2007, **111**, 11131–11138.
188 Y.-S. Hu, R. Demir-Cakan, M.-M. Titirici, J.-O. Müller, R. Schlögl, M. Antonietti and J. Maier, *Angew. Chem., Int. Ed.*, 2008, **47**, 1645–1649.
189 Y. Xu, G. Yin, Y. Ma, P. Zuo and X. Cheng, *J. Mater. Chem.*, 2010, **20**, 3216–3220.
190 H. Kim and J. Cho, *Nano Lett.*, 2008, **8**, 3688–3691.
191 B. Hertzberg, A. Alexeev and G. Yushin, *J. Am. Chem. Soc.*, 2010, **132**, 8548–8549.
192 L.-F. Cui, R. Ruffo, C. K. Chan, H. Peng and Y. Cui, *Nano Lett.*, 2009, **9**, 491–495.
193 G. Derrien, J. Hassoun, S. Panero and B. Scrosati, *Adv. Mater.*, 2007, **19**, 2336–2340.
194 C. M. Park and H. J. Sohn, *Chem. Mater.*, 2008, **20**, 3169–3173.
195 Z. Chen, Y. Cao, J. Qian, X. Ai and H. Yang, *J. Mater. Chem.*, 2010, **20**, 7266–7271.
196 M. G. Kim, S. Sim and J. Cho, *Adv. Mater.*, 2010, **22**, 5154–5158.
197 R. Hu, H. Liu, M. Zeng, H. Wang and M. Zhu, *J. Mater. Chem.*, 2011, **21**, 4629–4635.
198 H. Lee and J. Cho, *Nano Lett.*, 2007, **7**, 2638–2641.
199 S. Chen, P. Chen, M. Wu, D. Pan and Y. Wang, *Electrochem. Commun.*, 2010, **12**, 1302–1306.
200 P. Poizot, S. Laruelle, S. Grugeon, L. Dupont and J. M. Tarascon, *Nature*, 2000, **407**, 496–499.
201 X. Sun, J. Liu and Y. Li, *Chem. Mater.*, 2006, **16**, 3486–3494.
202 W.-M. Zhang, X.-L. Wu, J.-S. Hu, Y.-G. Guo and L.-J. Wan, *Adv. Funct. Mater.*, 2008, **18**, 3941–3946.
203 T. Muraliganth, A. V. Murugan and A. Manthiram, *Chem. Commun.*, 2009, (47), 7360.
204 (*a*) S. M. Yuan, J. X. Li, L. T. Yang, L. W. Su, L. Liu and Z. Zhou, *ACS Appl. Mater. Interfaces*, 2011, **3**, 705–709; (*b*) S. M. Yuan, Z. Zhou and G. Li, *CrystEngComm*, 2011, **13**, 4709–4713.
205 H. Qiao, Z. Zheng, L. Z. Zhang and L. F. Xiao, *J. Mater. Sci.*, 2008, **43**, 2778–2784.
206 J. S. Chen, Y. L. Cheah, Y. T. Chen, N. Jayaprakash, S. Madhavi, Y. H. Yang and X. W. Lou, *J. Phys. Chem. C*, 2009, **113**, 20504–20508.
207 R. Yang, W. Zhao, J. Zheng, X. Zhang and X. Li, *J. Phys. Chem. C*, 2010, **114**, 20272–20276.
208 X. W. Lou, D. Deng, J. Y. Lee and L. A. Archer, *Chem. Mater.*, 2008, **20**, 6562–6566.
209 X. W. Lou, C. M. Li and L. A. Archer, *Adv. Mater.*, 2009, **21**, 2536–2539.
210 Y.-S. Lin, J.-G. Duh and M.-H. Hung, *J. Phys. Chem. C*, 2010, **114**, 13136–13141.
211 L. Ji, Z. Lin, B. Guo, A. J. Medford and X. Zhang, *Chem.–Eur. J.*, 2010, **16**, 11543–11548.
212 P. Wu, N. Du, H. Zhang, J. X. Yu and D. R. Yang, *J. Phys. Chem. C*, 2010, **114**, 22535–22538.
213 J. Yan, A. Sumboja, E. Khoo and P. S. Lee, *Adv. Mater.*, 2011, **23**, 746–750.
214 S. Shanmugam, A. Gabashvili, D. S. Jacob, J. C. Yu and A. Gedanken, *Chem. Mater.*, 2006, **18**, 2275–2282.
215 C. Lai, H. Z. Zhang, G. R. Li and X. P. Gao, *J. Power Sources*, 2011, **196**, 4735–4740.
216 L. Liu, Y. Li, S. M. Yuan, M. Ge, M. M. Ren, C. S. Sun and Z. Zhou, *J. Phys. Chem. C*, 2010, **114**, 251–255.
217 S.-L. Chou, J.-Z. Wang, D. Wexler, K. Konstantinov, C. Zhong, H.-K. Liu and S.-X. Dou, *J. Mater. Chem.*, 2010, **20**, 2092–2098.
218 M. Y. Cheng and B. J. Hwang, *J. Power Sources*, 2010, **195**, 4977–4983.
219 S. Shanmugam and A. Gedanken, *J. Phys. Chem. B*, 2006, **110**, 24486–24491.
220 B. Sun, Z. Chen, H.-S. Kim, H. Ahn and G. Wang, *J. Power Sources*, 2011, **196**, 3346–3349.
221 L.-Y. Jiang, S. Xin, X.-L. Wu, H. Li, Y.-G. Guo and L.-J. Wan, *J. Mater. Chem.*, 2010, **20**, 7565–7569.
222 Z. Wang, J. S. Chen, T. Zhu, S. Madhavi and X. W. Lou, *Chem. Commun.*, 2010, **46**, 6906–6908.
223 X. Yu, S. Yang, B. Zhang, D. Shao, X. Dong, Y. Fang, Z. Li and H. Wang, *J. Mater. Chem.*, 2011, **21**, 12295–12302.
224 M. Pumera, *Energy Environ. Sci.*, 2011, **4**, 668–674.
225 L.-S. Zhang, L.-Y. Jiang, H.-J. Yan, W. D. Wang, W. Wang, W.-G. Song, Y.-G. G and L.-J. Wan, *J. Mater. Chem.*, 2010, **20**, 5462–5467.
226 S. L. Chou, J. Z. Wang, M. Choucair, H. K. Liu, J. A. Stride and S. X. Dou, *Electrochem. Commun.*, 2010, **12**, 303–306.
227 G. Wang, B. Wang, X. Wang, J. Park, S. Dou, H. Ahn and K. Kim, *J. Mater. Chem.*, 2009, **19**, 8378–8384.
228 P. Lian, X. Zhu, H. Xiang, Z. Li, W. Yang and H. Wang, *Electrochim. Acta*, 2010, **56**, 834–840; D. Y. Chen, G. Ji, Y. Ma, J. Y. Lee and J. M. Lu, *ACS Appl. Mater. Interfaces*, 2011, DOI: 10.1021/am200592r.
229 L. Ji, Z. Tan, T. R. Kuykendall, S. Aloni, S. Xun, E. Lin, V. Battaglia and Y. Zhang, *Phys. Chem. Chem. Phys.*, 2011, **13**, 7170–7177.
230 B. Li, H. Cao, J. Shao, M. Qu and J. H. Warner, *J. Mater. Chem.*, 2011, **21**, 5069–5075.
231 G. Zhou, D.-W. Wang, F. Li, L. Zhang, N. Li, Z.-S. Wu, L. Wen, G. Q. Lu and H.-M. Cheng, *Chem. Mater.*, 2010, **22**, 5306–5313.
232 X. Huang, X. Zhou, L. Zhou, K. Qian, Y. Wang, Z. Liu and C. Yu, *ChemPhysChem*, 2011, **12**, 278–281.
233 X. Meng, D. Geng, J. Liu, M. N. Banis, Y. Zhang, R. Li and X. Sun, *J. Phys. Chem. C*, 2010, **114**, 18330–18337.
234 Y. Li, X. Lv, J. Lu and J. Li, *J. Phys. Chem. C*, 2010, **114**, 21770–21774.
235 D. W. Choi, D. H. Wang, V. V. Viswanathan, I. T. Bae, W. Wang, Z. M. Nie, J. G. Zhang, G. L. Graff, J. Liu, Z. G. Yang and T. Duong, *Electrochem. Commun.*, 2010, **12**, 378–381.
236 K. Chang and W. Chen, *Chem. Commun.*, 2011, **47**, 4252–4254.
237 B. Li, H. Cao, J. Shao, G. Li, M. Qu and G. Yin, *Inorg. Chem.*, 2011, **50**, 1628–1632.
238 S. Q. Chen and Y. Wang, *J. Mater. Chem.*, 2010, **20**, 9735–9739.
239 B. Wang, X.-L. Wu, C.-Y. Shu, Y.-G. Guo and C.-R. Wang, *J. Mater. Chem.*, 2010, **20**, 10661–10664.
240 X. Zhu, Y. Zhu, S. Murali, M. D. Stoller and R. S. Ruoff, *ACS Nano*, 2011, **5**, 3333–3338.
241 J. Zhu, T. Zhu, X. Zhou, Y. Zhang, X. W. Lou, X. Chen, H. Zhang, H. H. Hng and Q. Yan, *Nanoscale*, 2011, **3**, 1084–1089.
242 H. Wang, L.-F. Cui, Y. Yang, H. S. Casalongue, J. T. Robinson, Y. Liang, Y. Cui and H. Dai, *J. Am. Chem. Soc.*, 2010, **132**, 13978–13980.
243 S. Yang, X. Feng, S. Ivanovici and K. Müllen, *Angew. Chem., Int. Ed.*, 2010, **49**, 8408–8411.
244 K. Wang, Z. Li, Y. Wang, H. Liu, J. Chen, J. Holmes and H. Zhou, *J. Mater. Chem.*, 2010, **20**, 9748–9753.
245 X. Zhou, F. Wang, Y. Zhu and Z. Liu, *J. Mater. Chem.*, 2011, **21**, 3353–3358.
246 L. Shen, C. Yuan, H. Luo, X. Zhang, S. Yang and X. Lu, *Nanoscale*, 2011, **3**, 572.
247 F.-Y. Su, C. You, Y.-B. He, W. Lv, W. Cui, F. Jin, B. Li, Q.-H. Yang and F. Kang, *J. Mater. Chem.*, 2010, **20**, 9644–9650.
248 D. Pan, S. Wang, B. Zhao, M. Wu, H. Zhang, Y. Wang and Z. Jiao, *Chem. Mater.*, 2009, **21**, 3136–3142.